Implementation of harmonic quantum transition state theory for multidimensional systems

Dóróthea Margrét Einarsdóttir

Faculty of Physical Sciences
University of Iceland
2010

IMPLEMENTATION OF HARMONIC QUANTUM TRANSITION STATE THEORY FOR MULTIDIMENSIONAL SYSTEMS

Dóróthea Margrét Einarsdóttir

90 ECTS thesis submitted in partial fulfillment of a
Magister Scientiarum degree in Chemistry

Advisor
Prof. Hannes Jónsson

Examinor
Andrei Manolescu

Faculty of Physical Sciences
School of Engineering and Natural Sciences
University of Iceland
Reykjavík, May 2010

Implementation of harmonic quantum transition state theory for multidimensional systems
Implementation of harmonic quantum TST
90 ECTS thesis submitted in partial fulfillment of a M.Sc. degree in Chemistry

Faculty of Physical Sciences
School of Engineering and Natural Sciences
University of Iceland
Hjarðarhagi 2-6
107 Reykjavík
Iceland

Telephone: 525 4000

Bibliographic information:
Dóróthea Margrét Einarsdóttir, 2010, Implementation of harmonic quantum transition state theory for multidimensional systems, M.Sc. thesis, Faculty of Physical Sciences, University of Iceland.

Printing: Háskólaprent, Fálkagata 2, 107 Reykjavík
Iceland, May 2010

Abstract

Calculation of the rate of atomic rearrangements, such as chemical reactions and diffusion events, is an important problem in chemistry and condensed matter physics. When light particles are involved, such as hydrogen, the quantum effect of tunneling can be dominating. Harmonic quantum transition state theory (HQTST), sometimes referred to as 'instanton theory', is analogous to the more familiar classical harmonic transition state theory (HTST) except that it includes the effect of quantum delocalization. In this thesis, a new method for finding quantum mechanical saddle points, or instantons, is presented. The method is based on finding the classical periodic orbits on the inverted potential by a path optimization method. A chosen number of the system replicas are distributed along a path to give a convenient numerical representation of the classical orbit, independent of the physical parameters. This is in contrast with the distribution according to equal time segments which places most replicas near the end points. The overall computational cost of estimating rate constants with this method is lower than in previously used formulations of HQTST which is especially important when using directly atomic forces obtained from first principles calculations where each evaluation of the energy and atomic forces usually is computationally demanding. The method was tested on several two dimensional models as well as a multi dimensional problem involving hydrogen molecule adsorption/desorption from a crystal surface, yielding results in excellent agreement with quantum rate constants calculated using full free energy calculations and previously published implementation of HQTST.

Contents

List of figures

Glossary

CLASSICAL DYNAMICS: The time evolution of Newton's equations for a classical system.

CFP: Closed Feynman path. The Feynman paths that are periodic in imaginary time, start and terminate at the same point. Since the quantum partition function is given by the trace of the density matrix, it is represented only with closed Feynman paths.

DFT: Density functional theory. An approximate method of solving Schrödinger's equation for a system of electrons. The energy and force of the system is calculated from the electron density. DFT scales better than many-body-orbital based quantum chemistry methods and can be used with larger systems.

EAM: Embedded atom method. A form of empirical potential function which quite accurately describes some metals including copper.

FEYNMANN PATH INTEGRAL: One formulation of quantum mechanics. The probability of a particle starting from a given configuration and ending at another some time later is given by an integral over all possible paths connecting the two configurations. In real time it describes quantum dynamics and in imaginary time, quantum statistical dynamics.

HTST: Harmonic transition state theory. A simplified form of the transition state theory in which the potential is assumed to be of harmonic form both at the minimum and at the saddle point. This is a good approximation at low enough temperature, unless quantum effects become important.

HESSIAN MATRIX: The matrix of force constants (second derivatives of the potential energy function). When this matrix is divided by the masses of the atoms, the eigenvectors are the normal modes of vibrations, and the eigenvalues are the square of the normal mode frequencies.

HQTST: Harmonic quantum transition state theory. Approximate quantum mechanical rate is obtained by expanding the Euclidean action around the instanton.

INSTANTON: The saddle point along the MAP, the CFP with highest action. A quantum analog to the classical saddle point in HTST.

MAP: Minimum action path. Optimal sequence of closed Feynman paths connecting the reactant and product states and passing through the instanton. The path has the highest statistical relevance in the quantum mechanical partition function since it represents the lowest action.

MAXIMUM TUNNELING PATH: A path between two points on a potential surface with minimum action and maximum tunneling probability. Typically found between classical turning points with the same energy.

MEP: Minimum energy path. A path between two points on a potential surface of the lowest possible energy. This path follows the direction of steepest descent.

NEB: Nudge elastic band. A method for finding the MEP between two points on a potential surface. A path of discrete images of a system are connected by springs (elastic band) and allowed to collectively relax. The nudging refers to the fact that the spring forces act only along the band, and the potential forces act only perpendicular to the band.

POTENTIAL ENERGY SURFACE: Each point in configuration space represents one configuration or position of the atoms in the system. For this position, there is a potential energy. The potential enrgy surface is the surface defined by the value of the potential energy at each point in configuration space.

QQ-HTST: Quasi-quantum HTST. A form of HTST where the quantum effect of zero point energy is included. The classical partition function is substituted with their quantum mechanical analogs.

SADDLE POINT: A point on a potential surface at which the force is zero and at which there is one negative curvature or unstable mode in the Hessian matrix.

SCT: Small curvature tunneling theory. A semi-classical approximation to compute the tunneling probability of a system. The effect of reaction path curvature is included in an effective reduced mass.

TRANSITION STATE: A bottle neck region which a system must cross in order to undergo a transition from a given initial state. The transition state has one less dimension than the full system.

TST: Transition state theory. A theory for calculating the rate at which a system leaves a given initial state through a bottle neck region.

WKB: Wentzel–Kramers–Brillouin theory. A semi-classical approximation to compute the tunneling probability of a system.

Acknowledgments

I would like to thank my advisor prof. Hannes Jónsson, for the guidance and great support through my studies and the work of this project, and my fellow research group member Andri Arnaldsson for all the help with calculations and computational and theoretical matters. I would also like to thank Finnbogi Óskarsson for his contribution to the project at early stages and all other members of the research group for helpful discussions and general support.

1 Introduction

The calculation of the rate of transitions such as chemical reactions or diffusion events is a common problem in theoretical chemistry and condensed matter physics. What changes during a transition from initial state to final state is the configuration of particles. In chemical reactions the configuration of atoms is changed from the reactant state R to the product state P. The interaction between the atoms can be obtained by solving the Schrödinger equation or from an otherwise determined potential energy function.

A transition, such as a typical chemical reaction, is a rare event, in the sense that it is many orders of magnitude slower than the vibrations of the atoms. It takes a large fluctuation of the energy, coming from the heat bath, in just the right coordinates for the system to be able to reach the transition state and proceed over to P. A direct simulation of the classical dynamics is therefor not useful. The most important theoretical approach in analyzing the rate of chemical reactions is the so called 'transition state theory' (TST). The main strength of TST is that the rate at which a transition takes place can be calculated statistically instead of dynamically, avoiding the time scale separation problem. The transition state is defined as a subspace that consists of a narrow region around a dividing surface representing a bottle neck for the transition of the system from R to P. It is the part of the reaction path where the probability of finding the system is particularly small and the width of this subspace is infinitesimal. The key approximation in TST is that if the system makes it to the transition state and is heading towards P, then we can assume that the system will end up in P for an extended time. In most cases, there is a natural separation of time scale. The time it takes the system to leave the transition state is very short compared with the time between thermally activated transitions from R to P or from P to R. For transitions in classical systems, the path with largest statistical weight is the minimum energy path (MEP) which can be represented as a chain of system replicas stretching from the reactant region to the product region in configuration space in such a way that the perpendicular force on each replica is zero and the replicas are connected together via springs obeying Hook's law. The MEP of a system can be found via the Nudge Elastic Band (NEB) method [1].

TST is inherently classical but quantum mechanical effects are especially important at low temperatures and when the transition involves light particles. Extensions of TST to quantum mechanical systems is still a matter of active research but two

types of effects are particularly important. The zero point energy effect displays in the fact that a quantum particle is delocalized and therefore cannot have the minimum potential energy. A stronger effect is when a quantum particle tunnels from one point on the potential energy surface to another. In such cases the system does not follow the minimum energy path, instead a so called tunneling path is the dominating path from a statistical view. In general, the tunneling path shortens the distance between R and P and lowers the activation energy. In this thesis the focus will be on methods for calculating the quantum mechanical rate constant, considering quantum effects, both tunneling and zero-pont energy. One of the most widely used method for approximating quantum mechanical rate constants is the harmonic quantum transition state theory (HQTST), or instanton theory, which is based on Feynman path integrals. It has shown to yield good approximations but in practice, when used with first principles calculations, it can require high computational effort. The aim of the work presented was to lower computational effort of quantum rate constant calculations, improvement of instanton theory showed to be most promising. In chapter 2 various methods for calculating rate constants will be reviewed. In chapter 3 a general path optimization method is proposed and applied to the case of tunneling paths. This path optimization represents an extension of the nudged elastic band method where endpoints can move freely along the energy contours and it is tested on different test examples in chapter 4. Comparison between rate constant calculations using different methods is given in chapter 5 and the resemblance of maximum tunneling paths and instantons is addressed in chapter 6, along with implementation of the tunneling path method to HQTST rate constant calculations.

2 Methods

2.1 Classical Transition State Theory

Consider a potential function $V(\mathbf{x})$ where two minimas represent the initial state R of the system and the final state P. If the transition state, with infinitesimal width σ, represents a tight bottle neck for going from R to P, then one can approximate the rate constant in a simple way, using the key assumption of TST, as a multiplication of the probability of making it to the transition state and the rate of crossing it from R to P

$$k^{TST} = \frac{\sigma \int_{\ddagger} e^{-V(\mathbf{x})/k_B T} d\mathbf{x}}{\int_R e^{-V(\mathbf{x})/k_B T} d\mathbf{x}} * \frac{< \upsilon_\perp >}{\sigma} \tag{2.1}$$

where $\ddagger$ denotes the transition state, $< \upsilon_\perp >$ is the average velocity in crossing the transition state, in a direction normal to the dividing surface and k_B is Boltzmann constant. If the system leaves the transition state in the direction towards the product region, P, it will continue to stay in the product region and spend an extended time there until another energy fluctuation takes it back to R. This is a good approximation if the dynamics are simple and the classical trajectories do not go back and forth over the dividing surface before landing in either R or P. The two other approximation in TST are the assumption that classical dynamics on the Born-Oppenheimer surface is a valid description of the dynamics, and that the reactant has reached equilibrium conditions, i.e. the energy in each degree of freedom is described by the Boltzmann distribution. For a typical transition rate, there is a very large number of vibrations in between reactive events, on the order of 10^{10}, so the last approximation is usually an excellent one.

Since the width of the transition state is infinitesimal, the potential energy can be taken to be constant in the direction normal to the dividing surface. The average velocity in crossing the transition state, $< \upsilon_\perp >$, can be calculated from the Maxwell distribution

$$< \upsilon_\perp > = \frac{\int_0^\infty \upsilon e^{-\sum_i \frac{1}{2}\mu_i \nu_i^2 / k_B T} d\nu}{\int_{-\infty}^\infty e^{-\sum_i \frac{1}{2}\mu_i \nu_i^2 / k_B T} d\nu} = \sqrt{\frac{k_B T}{2\pi\mu}} \tag{2.2}$$

Here μ is the effective mass for the motion across the transition state, a linear combination of the masses of the atoms that get displaced in the transition. The TST approximation to the rate constant can then be written as

$$k^{TST} = \sqrt{\frac{k_B T}{2\pi\mu}} \frac{Z^{\ddagger}}{Z^R} \tag{2.3}$$

where Z denotes the integral of the Boltzmann factor over the specified region of configuration space.

2.2 Harmonic Transition State Theory

For systems where the atoms are vibrating about fixed average positions, such as atoms in solids, or molecules reacting on the surface of a solid, the region of the potential surface that is of greatest importance can be represented by a harmonic approximation. For a diatomic molecule, the interaction potential, which is only a function of the distance between the atoms, can be expanded in Taylor expansion that gets truncated at the second power to give

$$V(r) \approx V(r_0) + \frac{1}{2}k(r - r_0)^2 \tag{2.4}$$

where r_0 is the distance at which the potential energy is minimal and $k = V''(r_0)$, also called force constant or spring constant as in Hook's spring force $F = -kx$. The generalization of this towards systems with more than one vibrational degree of freedom involves the calculation of mixed second derivatives but if one uses instead the coordinates corresponding normal modes of vibration, q_i, such mixed derivatives vanish since the normal modes are independent and do not mix within the harmonic approximation. The construction of the normal modes of vibration can be carried out for any point on the potential energy surface, in particular at the minimum corresponding to R. Since the force is zero at the minimum, the first derivative of the potential vanishes and the expansion of the potential is

$$V^R(\mathbf{q}) \approx V_{min} + \sum_{i=1}^{D} \frac{1}{2} k_i^R q_{R,i}^2 \tag{2.5}$$

in the region close to the minimum. Here V_{min} is the energy at the minimum, k_i^R are the force constants for each normal mode and D is the number of degrees of freedom. While this will not be a good approximation for regions far from the minimum, it is good enough if the potential energy is high enough in those regions so that the probability of finding the system there is insignificant.

If the dividing surface is chosen to lie along the potential energy ridge that separates the reactant state from the product state, then the most important point on the dividing surface, the point with largest statistical weight, is a saddle point. It is a minimum with respect to all the degrees of freedom within the dividing surface, but a maximum with respect to the motion normal to the dividing surface. If more than one saddle point exists on the potential energy ridge, the one with lowest energy is most important. For each low lying saddle point, one can carry out a second order Taylor expansion of the potential energy within the dividing surface

$$V^{\ddagger}(\vec{q}) \approx V_{SP} + \sum_{i=1}^{D-1} \frac{1}{2} k_i^{\ddagger} q_{\ddagger,i}^2 \tag{2.6}$$

where V_{SP} is the energy at the saddle point. The normal mode corresponding to motion normal to the dividing surface is not included so the number of normal modes is $D-1$. The width of the transition state, σ, is so small normal to the dividing surface that the potential is taken to be constant in that direction. With these approximation to the potential energy surface, the TST expression for the rate constant becomes the harmonic TST, HTST, approximation

$$k^{HTST} = \sqrt{\frac{k_B T}{2\pi\mu}} \frac{Z^{\ddagger}}{Z^R} = \sqrt{\frac{k_B T}{2\pi\mu}} \frac{e^{-V_{SP}/k_B T} \int_{-\infty}^{\infty} exp\left[-\sum_{i=1}^{D-1} \frac{1}{2} k_i^{\ddagger} q_{\ddagger,i}^2 / k_B T \right] d_{\ddagger,i}}{e^{-V_{min}/k_B T} \int_{-\infty}^{\infty} exp\left[-\sum_{i=1}^{D} \frac{1}{2} k_i^R q_{R,i}^2 / k_B T \right] dq_{R,i}} \tag{2.7}$$

For each one of the normal mode i, the integral over the Gaussian in equation 2.7 is

$$\int_{-\infty}^{\infty} e^{-\frac{1}{2} k_i q_i^2 / k_B T} dq_i = \sqrt{\frac{2\pi k_B T}{k_i}} \tag{2.8}$$

and the rate constant is

$$k^{HTST} = \sqrt{\frac{k_B T}{2\pi\mu}} \frac{\prod_{i=1}^{D-1} \sqrt{\frac{2\pi k_B T}{k_{\ddagger,i}}}}{\prod_{i=1}^{D} \sqrt{\frac{2\pi k_B T}{k_{R,i}}}} e^{-(V_{SP} - V_{min})/k_B T} \tag{2.9}$$

All the factors of $k_B T$ cancel out and all except one of 2π. Multiplying the square root of the effective mass in both the numerator and the denominator gives

$$k^{HTST} = \frac{1}{2\pi} \frac{\prod_{i=1}^{D} \sqrt{k_{R,i}/\mu}}{\prod_{i=1}^{D-1} \sqrt{k_{\ddagger,i}/\mu}} e^{-(V_{SP} - V_{min})/k_B T} \tag{2.10}$$

Recalling that the vibrational frequency is $\nu = \omega/2\pi = \frac{1}{2\pi}\sqrt{\frac{k}{\mu}}$ one yields

$$k^{HTST} = \frac{\prod_{i=1}^{D} \nu_{R,i}}{\prod_{i=1}^{D-1} \nu_{\ddagger,i}} e^{-(V_{SP}-V_{min})/k_B T} \tag{2.11}$$

Since only vibrational contributions to the partition function are to be considered equation 2.11 can be written in terms of the angular vibrational frequency, ω, of the reactant state and the saddle point.

$$k^{HTST} = \frac{1}{2\pi} \frac{\prod_{i=1}^{3N} \omega_i^R}{\prod_{i=1}^{3N-1} \omega_i^\ddagger} e^{-(V_{SP}-V_{min})/k_B T} \tag{2.12}$$

The number of atoms used is N and the imaginary frequency corresponding to the unstable vibrational mode at the saddle point is left out from the product in the denominator.

The HTST approximation agrees with the empirically observed Arrhenius expression for the temperature dependence of the rate constant, $k = Ae^{-E_a/RT}$, where E_a is the activation energy which is simply the potential energy difference between the saddle point and the minimum corresponding to the reactant region. The prefactor has to do with the vibrational entropy. If the vibrational frequencies are low at the saddle point compared to the minimum, corresponding to a wide mountain pass, the prefactor is large. On the other hand, if the potential energy rises quickly away from the saddle point within the dividing surface, quicker than the vicinity of the minimum, the prefactor is small.

2.3 quasi-quantum HTST

The classical treatment of the vibration of atoms is often not good enough at low temperatures. When considering the quantum effects one needs to take into account the zero point energy of the vibrational ground state and in some cases the probability of the system tunneling from the reactant configuration to the product configuration. The simplest inclusion of zero point energy can be made if the system is most likely in the lowest energy level both initially and at the transition state. To include the zero-point energy in the activation energy, the term $V_{min} - V_{SP}$ is replaced with

$$E_a = \left(V_{SP} + \sum_{i=1}^{D-1} \frac{h\nu_{\ddagger,i}}{2}\right) - \left(V_{min} + \sum_{i}^{D} \frac{h\nu_{R,i}}{2}\right) \tag{2.13}$$

Since there is one fewer vibrational mode at the saddle point than at the minimum, the addition of zero-point energy tends to reduce the energy barrier.

Another simple way to include quantum effects of zero-point energy in the HTST rate constant expression is to replace the classical harmonic partition function for each vibrational normal mode with the corresponding quantum mechanical partition function. Substitution in equation 2.12 gives

$$k^{\text{qq-HTST}}(T) = \frac{k_B T}{2\pi h} \frac{\prod_{i=1}^{3N} 2sinh(\hbar\omega_i^R/2k_BT)}{\prod_{i=1}^{3N-1} 2sinh(\hbar\omega_i^\ddagger/2k_BT)} e^{-(V_{SP}-V_{min})/k_BT} \tag{2.14}$$

This introduces the zero-point energy in a more self-consistent manner than simply adding it to the exponent but no tunneling has been accounted for. Inclusion of tunneling effects in rate constant calculations will be the topic of following sections.

2.4 Harmonic Quantum TST

Several versions of quantum mechanical TST have been proposed. The most widely used formulation is based on statistical Feynman path integrals. The method proposes a quantum analog to MEP, the minimum action path, MAP, defining the path of minimum Euclidean action where real time is rotated to imaginary time through Wick rotation. In Feynman's formalism for quantum statistical dynamics, a quantum partition function is the trace of the equilibrium, thermal density matrix[2, 3]. The density matrix is directly derived from the real-time propagator from quantum dynamics, which gives the amplitude for a system to go from q_1 to q_2 in time τ. The density matrix is

$$\rho(q_1, q_2, \tau) = \int e^{-S_E[q(\tau)]/\hbar} D[q_{1\to 2(\tau)}] \tag{2.15}$$

$D[q_{1\to 2(\tau)}]$ extends over all possible paths connecting q_1 and q_2 in imaginary time $\tau = \beta\hbar$. Each path is weighted by the exponent of the corresponding Euclidean action $S_E = \int_0^{\beta\hbar} H d\tau$ where H is the classical Hamiltonian. In the real time quantum dynamics, the action is a time line integral of the classical Lagrangian. When imaginary time is substituted for real time in the Lagrangian, two i will change the sign on the potential energy term, converting the Lagrangian to a Hamiltonian. By considering the trace of the density matrix, the quantum partition function is obtained as

$$Q = Tr(\rho(q_1, q_2, \beta\hbar)) \tag{2.16}$$

$$= \int e^{-S_E[q(\tau)]/\hbar} D[q_{1\to 1(\tau)}] \tag{2.17}$$

Since the trace operator Tr only acts on the diagonal of the density matrix, only closed paths are included. Thus the quantum partition function relies only on paths starting at configuration q_1, traveling along a path for $\beta\hbar$ time and returning to the point of origin. Each point on the MAP is such a path, called closed Feynman path (CFP). The path is described as a distribution or a chain of replicas of the system connected through Hook springs. The statistical mechanics of a quantum system is mathematically equivalent to classical statistical mechanics of a CFP. An effective temperature depended potential energy function is defined as[4, 5]

$$V_{\text{eff}}(\mathbf{q}, T) = \sum_{i=1}^{P} \left[\frac{1}{2} k_{\text{sp}}(T) \left| q_{i+1} - q_i \right|^2 + \frac{V(q_i)}{P} \right] \tag{2.18}$$

where P is the number of images and k_{SP} is the temperature dependent spring constant

$$k_{\text{sp}}(T) = \mu P \left(\frac{k_B T}{\hbar} \right)^2 \tag{2.19}$$

The CFP of maximum action along the MAP is a saddle point of this extended quantum mechanical energy surface and is called the instanton. This effective potential energy function is connected to the Euclidean action S_E through

$$\frac{S_E}{\hbar} = \frac{V_{\text{eff}}}{k_B T} \tag{2.20}$$

An schematic illustration of the CPF compared to a classical particle is presented in figure 2.1.

At low enough temperature, the effective potential will develop saddle points off the classical MEP which correspond to paths where thermally assisted tunneling is the dominant mechanism. At higher temperature the effective potential equals the classical potential as all the system replicas collapse to a single point in the coordinate space. The cross-over temperature, where tunneling starts to play a significant role can be estimated from the curvature of the MEP at the classical saddle point. If ω is the magnitude of the imaginary vibrational frequency of the unstable mode at the saddle point, the cross-over temperature is given by[6]

$$T_c = \frac{\hbar \omega}{2\pi k_B} \tag{2.21}$$

As in HTST, where the reaction rate is estimated by expanding the potential energy surface around the classical saddle point in a second order Taylor polynomial, the quantum mechanical rate can be obtained by expanding the effective potential around the instanton on the MAP to second order, analogous to saddle point expansion in HTST. The instanton rate constant, k_{ins}, is then given by[5, 7]

$$Q_R k_{\text{ins}} = \sqrt{\frac{S_0}{2\pi\hbar}} \frac{\hbar P}{k_B T \left| \prod_j' \lambda_j \right|} e^{V_{\text{eff}}(q_{\text{ins}})\hbar / k_B T} \tag{2.22}$$

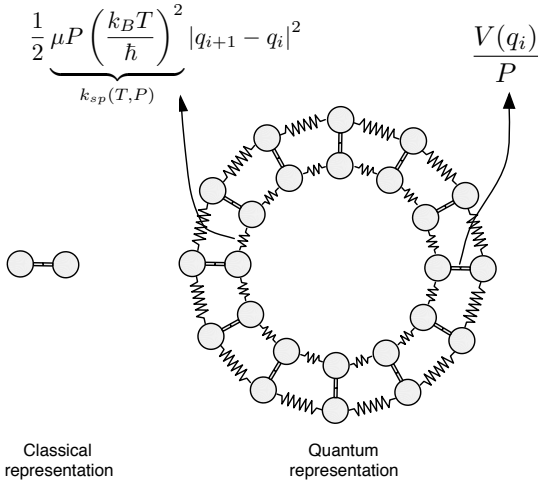

Figure 2.1: Schematic illustration of a closed Feynman path (CFP) for a diatomic molecule. The classical molecule is situated on the left hand side of the figure, the quantum mechanical CFP on the right. P is the number of system replicas (here P=12). The kinetic energy term is presented as springs with temperature dependent spring constants, k_{sp}, between the systems replicas where each atom is connected to itself in the neighboring replicas and the interatomic potential energy, within each replica, is scaled by the number of replicas. Given a high enough temperature the springs will contract the CFP to the classical configuration.

$V_{\text{eff}}(q_{\text{ins}})$ is the value of the effective potential at the instanton and S_0 is twice the instanton action due to the (imaginary-time) kinetic energy, or

$$S_0 = \frac{\mu P}{\beta\hbar}\sum_{j}^{P}|q_{j+1}-q_j|^2 \tag{2.23}$$

λ_j in equation 2.22 are the frequencies of the normal modes of vibration of the chain at the instanton. One vibrational mode has zero eigenvalue, namely the one corresponding to moving the images along the CFP or shifting labels. The prime on the product sign in equation 2.22 denotes the absence of the zero-mode.

2.5 Standard WKB method and Small Curvature Tunneling method

In TST the tunneling is often included by multiplying the rate constant computed with the usual classical treatment by a tunneling correction $\Gamma = k/k_{cl}$. This correction factor is a function of temperature and is defined as the ratio of the thermally

averaged quantum mechanical transmission probability, P(E), to the thermally averaged classical transmission probability for the same potential energy barrier.

$$\Gamma(T) = \frac{\int_0^\infty P(E)e^{-\beta E}dE}{\int_{V_{max}}^\infty e^{-\beta E}dE} \tag{2.24}$$

where V_{max} is the maximum of the potential energy barrier and $\beta = 1/k_BT$. The integral must extend up to infinity because the quantum correction must account for non classical reflection at energies above the barrier height as well as non classical transmission at energies below the barrier height [8].

Generally, the Wentzel–Kramers–Brillouin approximation[9, 10, 11], or WKB approximation is based on solving the Schrödinger equation by expanding the wave function in powers of $\hbar$. The one-dimensional WKB method is the most widely used semi-classical approximation to compute the tunneling probability. According to the method the semi classical approximation to the transmission probability for an energy E below the barrier height $V_{\max}$ is given by [12]

$$P(E) = \frac{1}{1 + e^{2\theta(E)}} \tag{2.25}$$

where the action integral θ is given by

$$\theta(E) = \frac{1}{\hbar}\int_{s_1}^{s_2} \sqrt{2\mu(V(s) - E)})ds \tag{2.26}$$

The classical turning points representing $V(s) = E$ are s_1 and s_2 and μ is the reduced mass for the motion along the reaction coordinate. For energies near and above the barrier height, $V_{\max}$, the turning points are purely imaginary. $\theta(E)$ is still given by equation 2.26 but the tunneling probability by [8]

$$P(E) = \begin{cases} (1 + exp[2\theta(E)])^{-1} & E_0 \leq E \leq V_{max} \\ 1 - (1 + exp[2\theta(2V_{max} - E_0)])^{-1} & V_{max} \leq E \leq 2V_{max} - E_0 \\ 1 & 2V_{max} - E_0 < E \end{cases} \tag{2.27}$$

Where E_0 is the threshold energy

$$E_0 = max[V(s = -\infty), V(s = +\infty)] \tag{2.28}$$

The rate constant can be evaluated from the tunneling probability through the correction factor but most often people are only interested in the temperature dependence so it is convenient to calculate the reactive flux, i.e. the multiple of the rate constant and the partition function Q_R [13]

$$Q_R k = \frac{1}{2\pi\hbar}\int_0^\infty P(E)e^{-\beta E}dE \tag{2.29}$$

and plotting a Arrhenius plot with $\ln(Q_R k)$ vs. 1/T displays the temperature dependence. As described here, the WKB method is a method for evaluating transmission through a one dimensional energy barrier. Various multidimensional WKB methods have been proposed [14, 15, 16] but will not be specially reviewed here. It is however possible to take a MEP of a two dimensional potential energy surface and treat it as a one dimensional barrier. This is done by defining the reaction coordinate as arc length of the MEP and present the barrier as a potential function of one variable. Although this is not the most accurate approximation in two dimensions since only one degree of freedom is taken into account it allows the use of this simple one dimensional method for higher dimensional cases.

Another method for calculating the quantum mechanical rate constant which also includes the effects of curvature along the reaction path is small curvature tunneling (SCT) approximation [17, 18]. It is based on considering a harmonic expansion of the potential energy surface written in terms of the reaction coordinate, s, and the 3N-1 orthonormal modes of vibration, centered along s,

$$V(s) = V_{MEP}(s) + \sum_{i=1}^{3N-1} \left(\frac{1}{2} + m_i\right) \hbar\omega_i(s) \tag{2.30}$$

where m_i is the vibrational state of mode i orthogonal to the MEP. Averaging the resulting Hamiltonian over the vibrational degrees of freedom introduces an effective tunneling mass into the one dimensional description of the system movement along the reaction coordinate. The effective tunneling mass can be interpreted in terms of the curvature along the reaction coordinate $\kappa(s)$ given by

$$\kappa(s) = \left(\sum_{i=1}^{F-1} [\kappa_i(s)]^2\right)^{1/2} \tag{2.31}$$

where the summation is over all generalized normal modes. $\kappa_i(s)$ is the reaction-path curvature component of mode i given by

$$\kappa_i(s) = -\mathbf{L}_i^T \mathbf{H} \frac{\nabla V}{|\nabla V|^2} \tag{2.32}$$

where $\mathbf{L}_i^T$ is the transpose of the generalized normal mode eigenvector of mode i, $\mathbf{H}$ is the Hessian matrix.

If $\mathbf{t}(s)$ is the distance from the tunneling path to the MEP in the direction of the curvature vector the effective mass is given as

$$\mu_{\text{eff}}(s) = \mu \left[(1 - |\kappa(s)\mathbf{t}(s)|)^2 + \left(\frac{d\mathbf{t}(s)}{ds}\right)^2\right] \tag{2.33}$$

The transmission probability $P(E)$ is calculated in the same way as in equation 2.25 with the imaginary action integral now dependent on this new effective tunneling mass $\mu_{\text{eff}}(s)$ instead of μ before. Ignoring the reaction path curvatures yields $\mu_{\text{eff}} = \mu$ and tunneling along the classical reaction coordinate is recovered. For large systems, this procedure is still prohibitively expensive.

3 Optimization of paths

The motivation for developing a path optimization method was to find a path on the potential energy surface with lowest action and highest tunneling probability. In section 3.1 this topic is further discussed but lets first consider the general representation. The method is based on a similar procedure as in the Nudge Elastic Band method (NEB) [1], where the result is a MEP between two given minimas on the surface. The path is composed of so called images with a specific coordinate vector $\mathbf{R}$ representing their position and the potential energy of each image is minimized, see reference [1] for more details. NEB has been shown to work in systems with many degrees of freedom so the following discussion is not restricted to dimensionality.

Now, in the general case, let's assume we have a function V of many variables and some functional $S(V)$. V could be a potential energy function or any other kind of a function of many variables. We want to find a path between some two points with values V_1 and V_2, call them s_1 and s_2 respectively, where this functional S is minimized. Before the optimization starts, we construct some path according to our initial guess and distribute a number of images along the path. Let the coordinate of each image be represented by a vector $\mathbf{R}_j$. The end points of the path, s_1 and s_2, do not have a given coordinate, only a given value of V so their position is optimized within corresponding equi-value contours.

Let's define the derivative of the functional with respect to position of each image j as

$$\boldsymbol{\phi}_j = -\frac{\partial S}{\partial \mathbf{R}_j} \tag{3.1}$$

$\boldsymbol{\phi}$ can be seen as a generalized force, analogous to the force $\mathbf{F} = -\nabla V$ in NEB. The object to be zeroed in the optimization is the component of $\boldsymbol{\phi}_j$ normal to path, denoted as $\boldsymbol{\phi}_j^{\perp}$. If $\widehat{\tau}_j$ is the unit tangent we can write

$$\boldsymbol{\phi}_j^{\parallel} = (\boldsymbol{\phi}_j \cdot \widehat{\tau}_j)\widehat{\tau}_j \tag{3.2}$$

$$\boldsymbol{\phi}_j^{\perp} = \boldsymbol{\phi}_j - \boldsymbol{\phi}_j^{\parallel} \tag{3.3}$$

The images can be distributed along the path in any way wanted, for example evenly distributed by string method [19] or by adding spring force between the images as in NEB. The parallel part of $\boldsymbol{\phi}$ is then replaced by a spring force defined as

$$\boldsymbol{\phi}_j^{sp} = k\left(|\mathbf{R}_{j+1} - \mathbf{R}_j| - |\mathbf{R}_j - \mathbf{R}_{j-1}|\right)\widehat{\tau}_j \tag{3.4}$$

where k is a spring constant and with vector summation we get the total effective $\boldsymbol{\phi}$:

$$\boldsymbol{\phi}_j^{\text{eff}} = \boldsymbol{\phi}_j^{\perp} + \boldsymbol{\phi}_j^{sp} \tag{3.5}$$

So far the equations resemble the NEB method but since in this case the end points do not have a fixed position they will also have to be minimized. However, the end images are only movable within their equi-value curve so the effective $\boldsymbol{\phi}_{0,n}$ is calculated a bit differently than $\boldsymbol{\phi}_j$ for intermediate images. The spring force component parallel to the gradient of V is projected out and instead a constraining force component is added. Let the derivative of V in each point be denoted as $\mathbf{F}_j = -\frac{\partial V}{\partial \mathbf{R}_j}$, the constraining force is then

$$(V(\mathbf{R}_{0,n}) - V_{1,2})\widehat{\mathbf{F}}_{0,n} \tag{3.6}$$

where the hat denotes unit vector. The generalized effective force to be zeroed on the end images is then a sum of the spring force normal to the gradient of V and the constraining force.

$$\boldsymbol{\phi}_{0,n}^{\text{eff}} = \boldsymbol{\phi}_{0,n}^{sp} - (\boldsymbol{\phi}_{0,n}^{sp} \cdot \widehat{\mathbf{F}}_{0,n})\widehat{\mathbf{F}}_{0,n} + (V(\mathbf{R}_{0,n}) - V_{1,2})\widehat{\mathbf{F}}_{0,n} \tag{3.7}$$

$\boldsymbol{\phi}_{\text{eff}}$ is then minimized to zero iteratively with respect to coordinates of all images using Quick-min[1] or other minimization methods.

As an example, the equations listed above were tested on a simple functional describing the distance between two energy points on a potential energy surface. The minimization yields the path with shortest distance between two energy values. The functional can be written as

$$S(\mathbf{R}) = \int_{s_1}^{s_2} d\mathbf{R} \approx \sum_{i=1}^{n} |\mathbf{R}_i - \mathbf{R}_{i-1}| \tag{3.8}$$

n being the number of images along the path between initial and final points, s_1 and s_2. Now differentiating the equation above gives

$$\boldsymbol{\phi}_j = -\frac{\partial S}{\partial \mathbf{R}_j} = -\frac{\mathbf{R}_j - \mathbf{R}_{j-1}}{|\mathbf{R}_j - \mathbf{R}_{j-1}|} + \frac{\mathbf{R}_{j+1} - \mathbf{R}_j}{|\mathbf{R}_{j+1} - \mathbf{R}_j|} \tag{3.9}$$

Following the outline of equations 3.2 to 3.7 and minimizing iteratively gives $\mathbf{R}$ for the path with shortest distance between two potential energy curves. This is illustrated in figure 3.1.

[1] A simple but quite efficient minimization method based on the Verlet algorithm for simulating classical dynamics[20]. At each timestep the coordinates and velocities are updated from the coupled first order equations of motion based on the force evaluated at the current coordinates. If the velocity is zeroed at each step, the algorithn gives a steepest descent minimization.

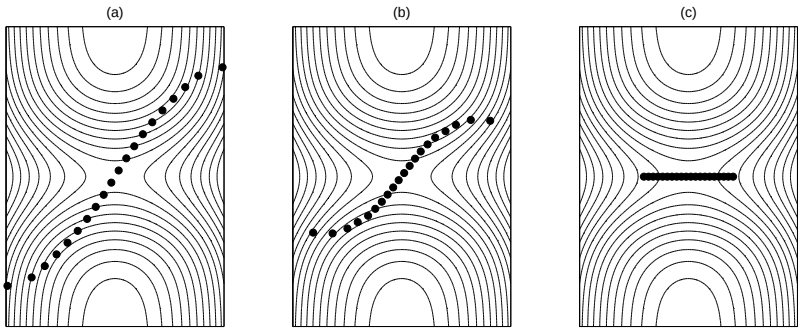

Figure 3.1: Illustration of the path optimization method. (a) shows an initial path between two potential energy points, (b) shows a intermediate step in the minimization of distance and (c) shows the final path with shortest distance between the equipotential curves.

3.1 Maximum tunneling paths

The maximum tunneling path is defined as a path between corresponding classical turning points for each different cross-over energy, where the action is minimized. These maximum tunneling paths differ from the classical MEP, they should represent minimum action and can therefore be described as classical periodic orbits for the inverted potential corresponding to a specific energy, see appendix A for more details. Note that in discussion of a maximum tunneling path only half a orbit is considered because it is totally symmetric, i.e. the system will turn around, so to speak, at the end point of the maximum tunneling path and return to its origin to complete a whole orbit, following the same path.

The optimization procedure described in the previous section can be used to find maximum tunneling paths between various classical turning points s_1 and s_2. The functional in this case is the action integral θ in equation 2.26, written now as a function of the coordinate vector $\mathbf{R}$ for one particular cross-over energy $\mathrm{E_c}$.

$$\theta(\mathbf{R}) = \frac{1}{\hbar}\int_{s_1}^{s_2} \sqrt{2\mu(V(\mathbf{R}) - E_c)}d\mathbf{R} \tag{3.10}$$

Minimizing this functional yields a path corresponding to the lowest action integral and hence the highest tunneling probability. Note that although the mass is simply noted here as μ, for multi dimensional systems the mass can be different for each coordinate and an effective reduced mass in each point on the path is possible to write

as a weighted average of the individual masses with respect to tangent components [21]. Lets start with using the Trapezoidal rule

$$T_n = \sum_{i=1}^{n} \frac{1}{2} \left(f(x_i) + f(x_{i-1}) \right) |x_i - x_{i-1}| \tag{3.11}$$

to approximate the integral in equation 3.10

$$\theta(\mathbf{R}) \approx \frac{1}{2\hbar} \sum_{i=1}^{n} \left(\sqrt{2\mu(V(\mathbf{R}_i) - E_c)} + \sqrt{2\mu(V(\mathbf{R}_{i-1}) - E_c)} \right) |\mathbf{R}_i - \mathbf{R}_{i-1}| \tag{3.12}$$

Defining a new function

$$\xi_i = \frac{1}{\hbar} \sqrt{2\mu(V(\mathbf{R}_i) - E_c)} \tag{3.13}$$

with the unit of 1/length, simplifies the equation and gives

$$\theta(\mathbf{R}) \approx \frac{1}{2} \sum_{i=1}^{n} (\xi_i + \xi_{i-1}) |\mathbf{R}_i - \mathbf{R}_{i-1}| \tag{3.14}$$

Differentiating the above equation with respect to the position of j$^{\text{th}}$ image then gives $\boldsymbol{\phi}$ as in eq. 3.1

$$\begin{aligned} \boldsymbol{\phi}_j = -\frac{\partial \theta}{\partial \mathbf{R}_j} &= -\frac{1}{2} \left\{ \frac{\mu \frac{\partial V}{\partial \mathbf{R}_j}}{\hbar^2 \xi_j} |\mathbf{R}_j - \mathbf{R}_{j-1}| + (\xi_j + \xi_{j-1}) \frac{\mathbf{R}_j - \mathbf{R}_{j-1}}{|\mathbf{R}_j - \mathbf{R}_{j-1}|} \right. \\ &\quad \left. + \frac{\mu \frac{\partial V}{\partial \mathbf{R}_j}}{\hbar^2 \xi_j} (\xi_{j+1} + \xi_j) \frac{\mathbf{R}_{j+1} - \mathbf{R}_j}{|\mathbf{R}_{j+1} - \mathbf{R}_j|} (-1) \right\} \end{aligned} \tag{3.15}$$

Now defining

$$\mathbf{d}_j = \mathbf{R}_j - \mathbf{R}_{j-1} \tag{3.16}$$

$$d_j = |\mathbf{d}_j| \tag{3.17}$$

$$\widehat{\mathbf{d}}_j = \frac{\mathbf{d}_j}{d_j} \tag{3.18}$$

and using the fact that the potential force on j$^{\text{th}}$ image is $\mathbf{F}_j = -\frac{\partial V}{\partial \mathbf{R}_j}$, equation 3.15 is simplified

$$\begin{aligned} \phi_j &= \frac{\mu}{2\hbar^2 \xi_j} \mathbf{F}_j d_j - \frac{(\xi_j + \xi_{j-1})}{2} \widehat{\mathbf{d}}_j + \frac{\mu}{2\hbar^2 \xi_j} \mathbf{F}_j d_{j+1} + \frac{(\xi_{j+1} + \xi_j)}{2} \widehat{\mathbf{d}}_{j+1} \\ &= \frac{\mu}{2\hbar^2 \xi_j} (d_j + d_{j+1}) \mathbf{F}_j - \frac{(\xi_j + \xi_{j-1})}{2} \widehat{\mathbf{d}}_j + \frac{(\xi_{j+1} + \xi_j)}{2} \widehat{\mathbf{d}}_{j+1}. \end{aligned} \tag{3.19}$$

Following the outline of equations 3.2 to 3.7, the generalized effective force $\boldsymbol{\phi}^{\text{eff}}$ is established for all images along the path between the classical turning points. Quickmin iterations yield the maximum tunneling path, i.e. the coordinate vector $\mathbf{R}$ with the lowest possible value of θ and the highest value of tunneling probability P. To illustrate the iteration procedure a plot of θ and $\boldsymbol{\phi}_{\text{eff}}$ versus number of iterations is shown in figure 3.2 along with a graph of θ vs. a shift in the tunneling path to emphasize that it is in fact the minima.

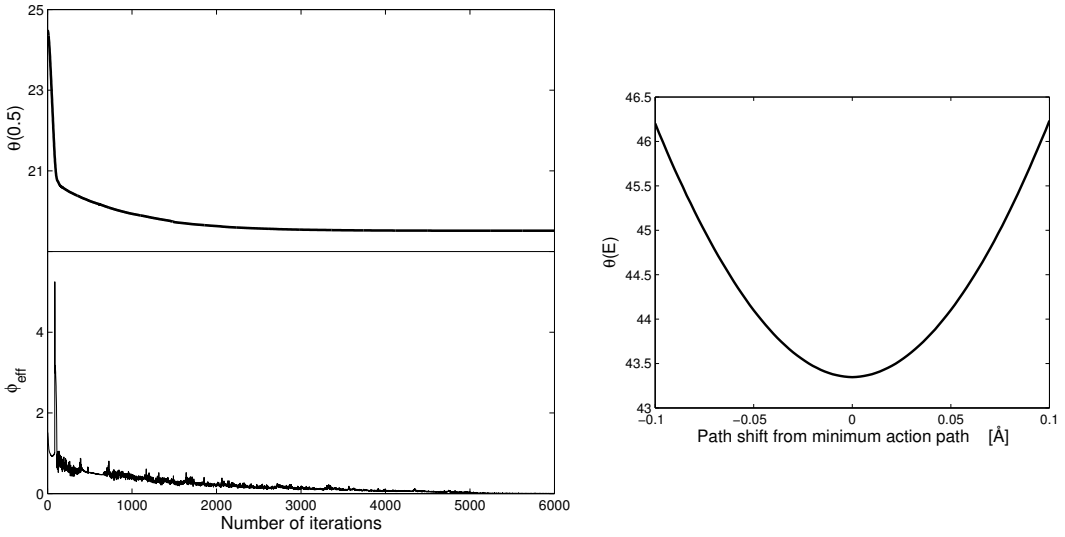

Figure 3.2: Above: Convergence of the value of θ for energy $E = 0.5$ as a function of the number of iteration. Below: Convergence of the maximum value of $\boldsymbol{\phi}_{eff}$ for the same minimization as a function of the number of iterations, converges to zero as expected. Right: The value of minimization object θ vs. a shift in the path, the path obviously corresponds to minimum value as intended.

As mentioned above, the calculation of a maximum tunneling path should give the same result as finding a periodic orbit for the inverted potential energy function -V($\mathbf{R}$) using classical dynamics. To test the result of the optimization procedure, classical dynamics were run on an inverted potential for a test example case, using the Verlet algorithm [20]. The initial point was chosen to be the same as an arbitrary tunneling path and the trajectory corresponding to a classical periodic orbit was found. An example is presented in figure 3.3 showing both the maximum tunneling path and the result of classical dynamics calculations when the initial point is chosen the same as the tunneling path's.

As expected, the paths are the same. However, finding the classical periodic orbit using classical dynamics of the Verlet algorithm requires extremely high accuracy of the initial position coordinates. For example, when finding the path in figure 3.3 for E_c=0.20eV a total of 10 correct digits in the initial position vector was necessary to get a proper path of a whole orbit with conservation of energy. Even more accu-

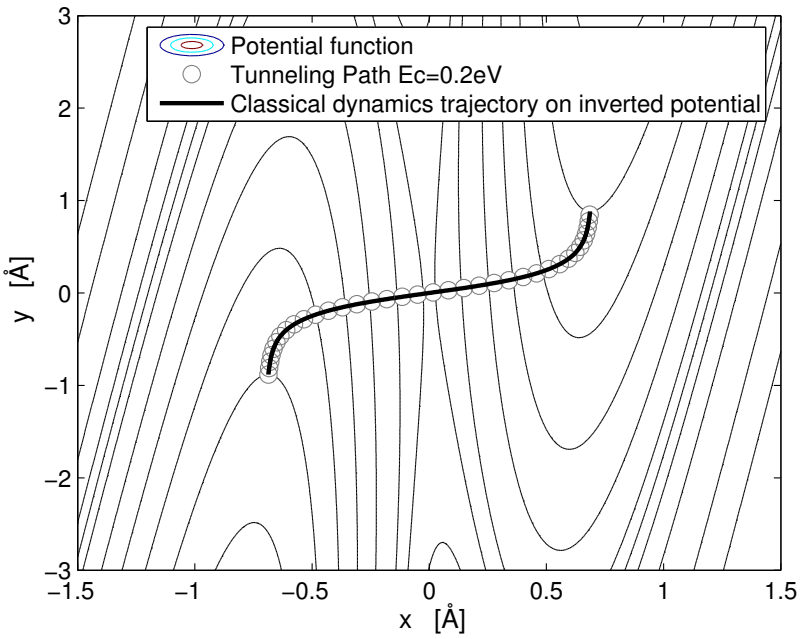

Figure 3.3: The classical periodic orbit shown in the figure can be calculated either by running classical dynamics trajectories on the inverted potential or by finding the maximum tunneling path with the optimization method. Both results are shown in the figure along with a contour plot of the potential function.

racy, is required for lower energies, for example over 60 digits for E_c=0.10eV. Such accuracy in position of the path has however no effect on rate constant estimation and the tunneling paths offer therefore a much cheaper way of finding these paths for rate constant calculations.

4 Test models

Various test model potential functions are presented in this chapter, some of them represent a physical model but others were designed only to emphasize different aspects of the resulting maximum tunneling paths. Maximum tunneling paths were found for all these test potential as described in following sections and rate calculations were also performed and are addressed in chapter 5 and 6. The paths are energy dependent and can be found for all energies where there is a chance of tunneling, starting from the energy of the state with higher potential up to the barrier height.

4.1 Symmetric Eckart barrier coupled to a harmonic oscillator

The first two dimensional model to be considered as a test example is the so called Eckart potential coupled to a harmonic oscillator. This model was constructed to describe a reaction in solution with a single solute coordinate coupled to a solvent represented by a harmonic oscillator. The potential function consists of a symmetric Eckart barrier along the solute coordinate x with a single harmonic oscillator bath, y, linearly coupled through a coupling constant to the solute reaction coordinate. This model system has been used in the past to make critical comparisons of approximate and accurate quantum mechanical calculations of the rate constants [22].

The potential energy function has a rather simple form:

$$V(x,y) = V_o sech^2(\alpha x/2) + \frac{1}{2}\mu\omega^2(y - Cx)^2 \tag{4.1}$$

The parameters are chosen $V_o = 0.425eV$, $\alpha = 3.97$Å, $\mu = 0.672amu$ and $\omega = 0.092\tau^{-1}$ and are meant to mimic a H+H_2 gas-phase reaction. The coupling constant C represents the linear response of a Gaussian friction kernel and is calculated by

$$C = \frac{4f\omega_x}{\pi\omega} e^{-\pi^2/32} \tag{4.2}$$

where ω_x is the magnitude of the imaginary angular frequency at the top of the Eckart barrier, ω is the angular frequency of the harmonic oscillator and f is a

dimensionless friction parameter. Here the coupling constant is chosen to be $C = 10.0$. The base units used in this model are eV for energy, Å for length, amu for mass, K for temperature and $\tau = 10.18$fs for time. A contour plot of the potential energy surface along with the classical MEP, traced out by NEB, and a tunneling path is shown in figure 4.1.

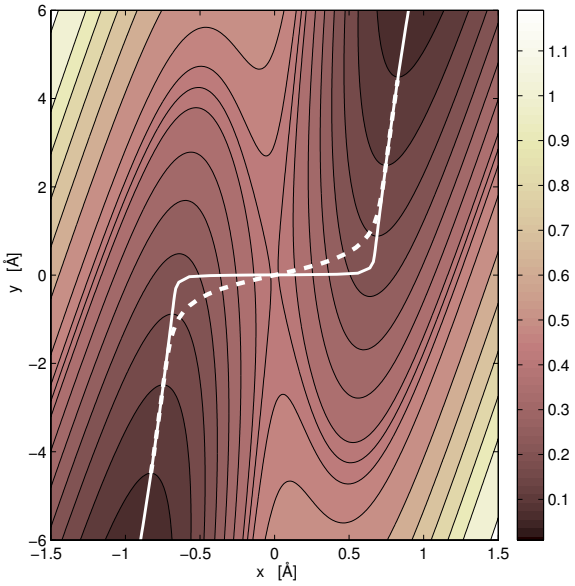

Figure 4.1: Eckart+HO potential function with MEP shown as a white solid line and a maximum tunneling path with cross over energy Ec=0.1eV shown as a dashed line.

4.1.1 Zero-point energy correction

This potential function is especially interesting when considering the quantum effect of zero-point energy. The first and most simplest quantum correction one could think of doing when treating a two dimensional potential function and its MEP is to do a harmonic expansion normal to the path in each point along the path and adding the zero-point energy, $\hbar\omega/2$, to the potential energy of the path. The expansion normal to and around a point r_0 on the path yields

$$V(r) = V(r_0) + (r - r_0)^2 \left.\frac{\partial^2 V}{\partial r^2}\right|_{r=r_0} = V(r_0) + \mu\omega^2(r - r_0)^2 \tag{4.3}$$

where r is the coordinate normal to the MEP. Note that the first derivative is zero. The vibrational frequency at each point r_0 on the path, $\omega(r_0)$, is then calculated by

$$\omega(r_0) = \sqrt{\frac{1}{\mu}\frac{\partial^2 V}{\partial r^2}}\bigg|_{r=r_0} \tag{4.4}$$

The results of adding the zero-point energy to the MEP are shown in figure 4.2. As

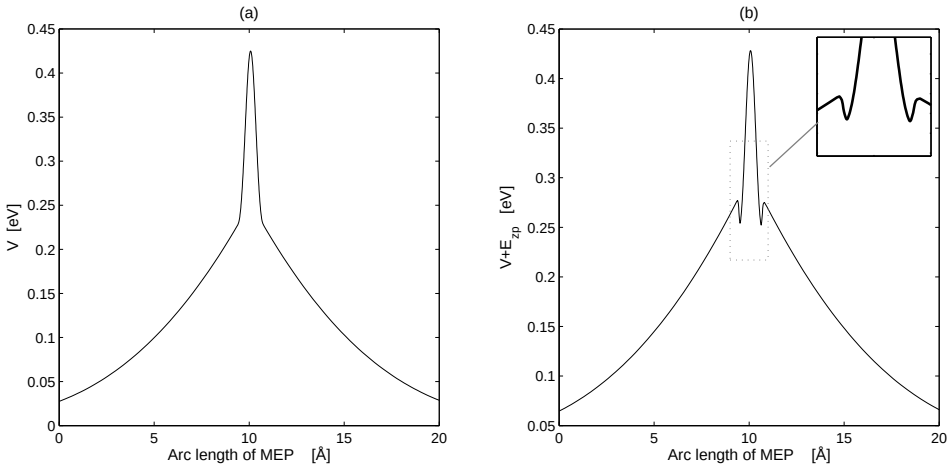

Figure 4.2: Eckart+HO potential barrier as a function of arc length. (a) shows the MEP barrier and (b) shows the barrier after addition of zero-point energy.

can be seen in the figure, the shape of the potential energy barrier is changed after adding the zero-point energy. Two local minimas appear at the 'corners' position on the MEP. The vibrational frequency is increasing from the initial point, and the potential valley is narrowing, up to the point where the MEP starts to curve significantly. Then the frequency decreases rapidly and the valley gets even wider at the saddle point than in the initial state. These drastic changes in ω cause the appearance of the two minimas in figure 4.2b. From this it is obvious that adding the zero-point energy to the potential along the path would not give a relativistic picture of the quantum effect.

4.2 Electron scattered by embedded Gaussian peaks in a parabolic potential

The second two dimensional model considered is an electron traveling through a quantum nanowire with embedded impurities in zero magnetic field. Numerical as well as theoretical studies have previously been performed on electron conductance

in such a wire [23, 24, 25]. The potential energy function constructed to describe the system is composed of two independent components.

$$V(x,y) = \frac{1}{2}m\omega^2 x^2 + \sum_{i=1}^{N} V_i e^{-\beta_i^2(x-x_i)^2+(y-y_i)^2)} \tag{4.5}$$

The wire is described to be of infinite length but parabolically confined along the transverse direction, and the scattering potential is chosen to be one or two Gaussians. The potential parameters are chosen to mimic the GaAs semi-conductor system as much as possible, $m = 0.067m_e$, $\omega = 3.04 \cdot 10^{12}s^{-1}$ and the barrier height is $V_o = 4.0meV$. In the case of a single Gaussian barrier situated at the center of the wire $\beta = 0.012247nm$, $x_1 = z_1 = 0.0nm$ and when considering two Gaussian barriers they are symmetrically offset around the center with $\beta = 0.031623nm$, $x_1 = z_1 = 20nm$ and $x2 = z_2 = -20nm$. The base units used in this model are meV for energy, 10nm for length, 0.067me for mass, K for temperature and $\tau' = 195.176$fs for time. A contour plot of the two potential surfaces is shown in figure 4.3.

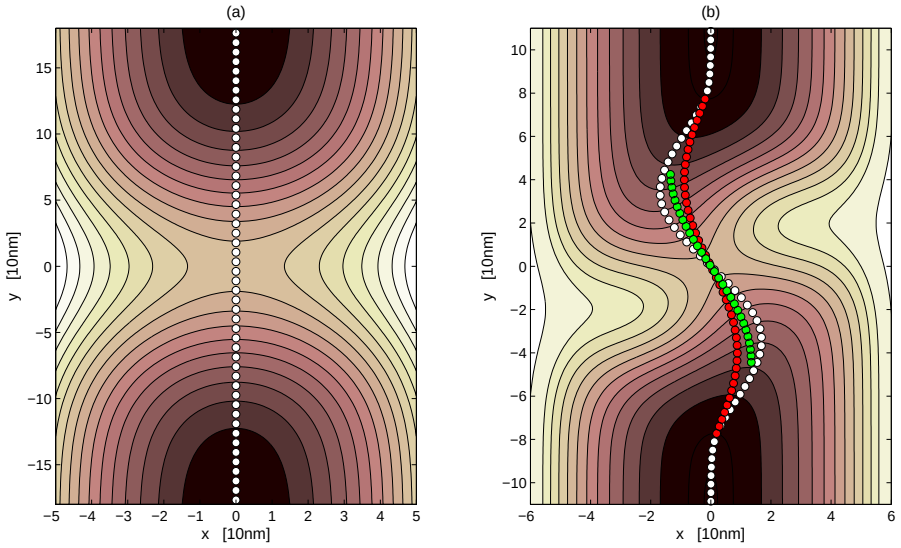

Figure 4.3: Potential surfaces for electron traveling along a model quantum nanowire with embedded impurity. A single Gaussian impurity on the left and two symmetrically offset impurities on the right. Also shown are the two different MEP and maximum tunneling paths for the second potential with $E_{cross} = 0.10meV$ and $E_{cross} = 1.10meV$.

Maximum tunneling paths were calculated for all energies up to the barrier height in the case of the two Gaussian potential, examples of two paths are shown in figure 4.3b where the corner cutting of the MEP (found with NEB) is obvious. The corner cutting is most extreme for low cross over energies, at energies near the barrier height $V_{\max}$ they only differ slightly from the MEP. In the case of the one Gaussian

potential the MEP is as straight line so no corner cutting is possible, however, any calculation of the rate constant using the MEP should give an insight to the effect of MEP curvature.

4.3 A simple LEPS potential coupled to a harmonic oscillator

This model represents a system of four atoms where an atom B can form a chemical bond with either one of two fixed atoms, A or C, and is simultaneously coupled in a harmonic way to a fourth atom D. This type of model has frequently been used as a simple representation of an activated process coupled to a medium, such as a chemical reaction in a liquid solution or in a solid matrix.

The reaction involving three atoms A, B and C confined to motion along a line can be described with the LEPS potential [26]. Only one bond can be formed, either between atoms A and B or between atoms B and C. The horizontal coordinate x is the distance between A and B and the vertical coordinate y is the distance between B and C.

$$\begin{aligned} V^{LEPS}(r_{AB}, r_{BC}) &= \frac{Q_{AB}}{1+a} + \frac{Q_{BC}}{1+b} + \frac{Q_{AC}}{1+c} - \left[\frac{J_{AB}^2}{(1+a)^2} + \frac{J_{BC}^2}{(1+b)^2} + \frac{J_{AC}^2}{(1+c)^2} \right. \\ &\quad \left. - \frac{J_{AB}J_{BC}}{(1+a)(1+b)} - \frac{J_{BC}J_{AC}}{(1+b)(1+c)} - \frac{J_{AB}J_{AC}}{(1+a)(1+c)} \right]^{\frac{1}{2}} \end{aligned} \tag{4.6}$$

The Q functions represent Coulomb interactions between the electron clouds and the nuclei and the J functions represent the quantum mechanical exchange interactions. The form of these functions is

$$Q(r) = \frac{d}{2}\left(\frac{3}{2} e^{2\alpha(r-r_0)} - e^{-\alpha(r-r_0)} \right) \tag{4.7}$$

and

$$J(r) = \frac{d}{4}\left(e^{2\alpha(r-r_0)} - 6e^{-\alpha(r-r_0)} \right) \tag{4.8}$$

The parameters are chosen to be $a = 0.05$, $b = 0.80$, $c = 0.05$, $d_{AB} = d_{BC} = 4.746$, $d_{AC} = 3.445$, $r_0 = 0.742$ and $\alpha = 1.942$.

Now the location of the end point atoms A and C is is fixed, allowing only atom B to move, and an additional degree of freedom is introduced. This can be interpreted as a fourth atom D which is coupled in a harmonic way to atom B.

$$V(r_{AB}, r_{BD}) = V^{LEPS}(r_{AB}, r_{AC} - r_{AB}) + 2k_c \left(r_{AB} - \left(\frac{r_{AC}}{2} - \frac{x}{c} \right) \right)^2 \tag{4.9}$$

where $r_{AC} = 3.742$, $k_c = 0.2025$ and $c = 1.154$. The base units used in this model are eV for energy, Å for length, amu for mass, K for temperature and $\tau = 10.18$fs for time. A contour plot of the potential function is shown in figure 4.4 along with examples of maximum tunneling paths.

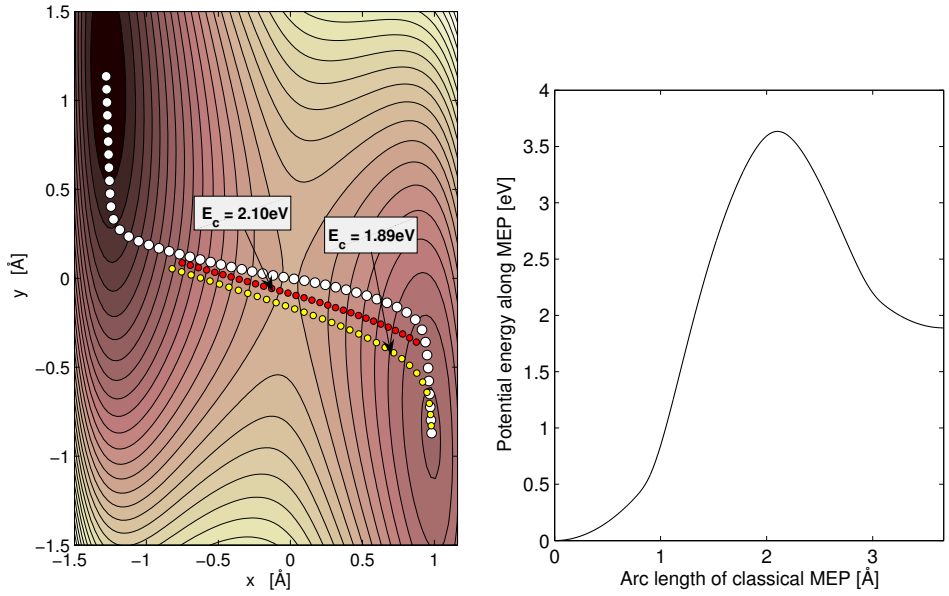

Figure 4.4: LEPS+HO potential energy surface is shown on the left as a contour plot and the classical MEP as a white dotted line between the two minimas. Also shown are two tunneling paths, one corresponding to cross-over energy 2.10eV and the other to 1.89eV. On the right is the one dimensional classical MEP barrier.

The LEPS+HO potential is an asymmetric potential and the product state is 1.89eV higher than the reactant state. Maximum tunneling paths were calculated for energies from 1.89eV up to the height of the barrier, $V_{\max} = 3.64eV$. In fig 4.4 the shift of the end points position of the path away from the MEP is quite obvious, the shift is larger for lower energies and smaller for higher energies.

4.4 Large corner cutting effect

A model was constructed to give an example of a system were the maximum tunneling paths would yield a large corner cutting of the MEP. The potential energy function is composed of two parabolic components and three Gaussian components.

$$V(x,y) = \frac{k_x}{2}x^2 + \frac{k_y}{2}y^2 + \sum_{i=1}^{3} \beta_i e^{-\alpha\left((x-x_i)^2+(y-y_i)^2\right)} \tag{4.10}$$

The parameters chosen are shown in table 4.1.

Table 4.1: Parameters used for test example potential.

$x_1 = 1.5$Å	$y_1 = 0.9$Å	$\beta_1 = \frac{k_x}{2}x_1^2 + \frac{k_y}{2}y_1^2$
$x_2 = 0.8$Å	$y_2 = -1.2$Å	$\beta_2 = \frac{k_x}{2}x_2^2 + \frac{k_y}{2}y_2^2$
$x_3 = 0.0$Å	$y_3 = 0.0$Å	$\beta_3 = 0.5$eV
$k_x = 4.0\text{eV/Å}^2$	$k_y = 3.0\text{eV/Å}^2$	$\alpha = 2.5$Å

The base units used in this model are eV for energy, Å for length, amu for mass, K for temperature and $\tau = 10.18$fs for time. A contour plot of the potential energy surface along with the classical MEP and examples of tunneling paths is shown in figure 4.5. The classical MEP barrier is asymmetric in shape and the product state is slightly lower in energy than the reactant state.

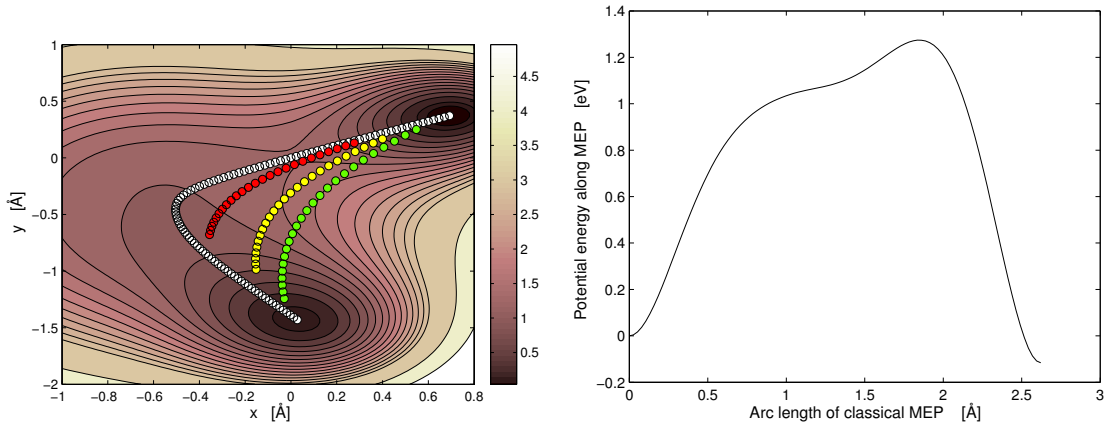

Figure 4.5: On the left is a contour plot of a potential function designed to yield large corner cutting. Also shown are the classical MEP (white dotted line) and three tunneling paths corresponding to different cross-over energies (green=0.2eV, yellow=0.7eV and red=1.0eV). On the right is a one dimensional plot of the classical MEP barrier.

As intended the maximum tunneling paths reduce the curvature significantly and also shorten the distance between initial and final state. The asymmetry of the surface also results in quite large shifting of end points, as they also differ quite from the MEP.

4.5 Constant MEP curvature

To investigate further the effect of MEP-curvature and vibrational frequency normal to MEP a model was proposed where the curvature of the MEP is constant. The shape of the MEP was chosen to be a half circle and the potential energy barrier as a function of arc length has the form of a Gaussian. Normal to the MEP the potential is a a parabola in the form of a harmonic oscillator with constant vibrational frequency along the path. The potential is a sum of two components a harmonic oscillator component and a Gaussian component. If the center of the circle is at (x_0, y_0) the distance from the center to each point on the surface is

$$s = \sqrt{(x - x_0)^2 + (y - y_0)^2} \tag{4.11}$$

If R is the radius of the MEP circle then the minimum distance from each point on the surface to a point on the MEP is $r_m = s - R$. The harmonic oscillator part of the potential is written

$$V_{HO}(x, y) = \frac{m\omega^2}{2} r_m^2 \tag{4.12}$$

where ω is the angular frequency and m is the mass of the particle taking part in the transition. The angle from the center of the circle can be written

$$T = \arcsin\left(\frac{y - y_0}{s}\right) \tag{4.13}$$

and the arc length of MEP is $q = (T\pi/2)R$ so the Gaussian component of the potential function can be written

$$V_G(x, y) = V_0 e^{-aq^2} \tag{4.14}$$

where V_0 is the maximum height of the barrier and a is a parameter controlling the width of the barrier. The total potential is then a sum of the two components

$$V(x, y) = V_{HO} + V_G = \frac{m\omega^2}{2} r_m^2 + V_0 e^{-aq^2} \tag{4.15}$$

The parameters were chosen to be $x_0 = 0.0$Å, $y_0 = -2.0$Å, $R = 2$Å, $\omega = 1.1\tau^{-1}$, $V_o = 0.62eV$, $a = 2/$Å^2 and $\mu = 0.672amu$. A contour plot of the potential along with it's MEP along with an example of a maximum tunneling path is shown in figure 4.6. The base units used in this model are eV for energy, Å for length, amu for mass, K for temperature and $\tau = 10.18$fs for time.

The maximum tunneling paths yield severe corner cutting of the circle-shaped MEP. In this case the shifting of end points from the MEP occurs mostly when the cross-over energy is high, as opposed to the models in two previous sections.

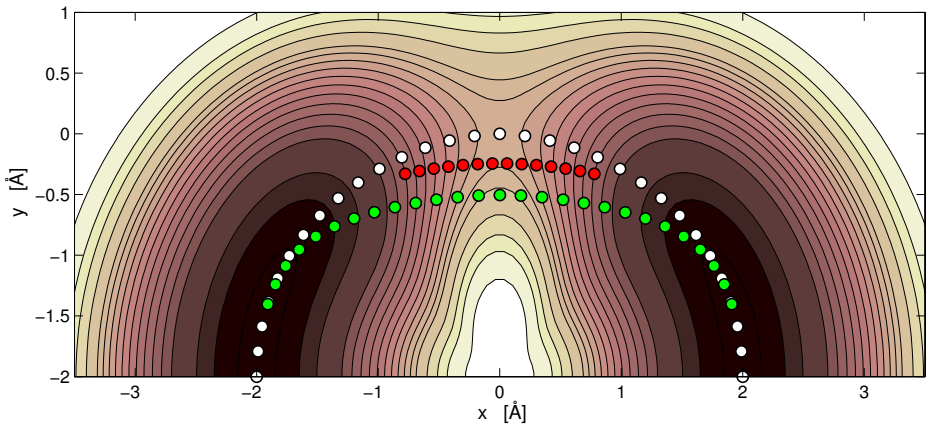

Figure 4.6: A contour plot of a potential function where the MEP has the shape of a half circle. Also shown are examples of maximum tunneling paths with cross-over energy E_c=0.001eV (green) and E_c=0.300eV (red).

4.6 Associative desorption of a hydrogen molecule from a Cu(110) surface

The last analytical potential energy function presented in this thesis as a test model is the associative desorption of a H_2 molecule from a Cu(110) surface. Both experimental and quantum calculations indicate unambiguous deviation from the classical Arrhenius law at lower temperatures [27]. Results of calculations of this system using an empirical many-body EAM potential have been published, where the potential form include a pair potential term for the screened Coulomb repulsion interaction between ions and a term for each ion embedded into a valence electron density of its neighboring ions [4, 28]. The system used here is the same as in references [4, 29] and consists of 216 Cu atoms representing the (110) surface. The Cu atoms are separated into 6 layers, each containing 36 atoms. The EAM potential gives the energetically most favorable configuration of the hydrogen atoms on the surface as aligned symmetrically along a surface valley, separated by a long bridge. The energy of the transition state lies 0.544eV above the energy of the adsorbed state. The MEP has been traced out by the NEB method and is depicted in figure 4.7 along with the tunneling paths of the hydrogen atoms.

The MEP is completely contained within a plane spanned by the initial, transition and final state and is symmetric about a plane parallel to the surface normal, orthogonal to the MEP plane and intersecting the transition state. The movement of the surface Cu atoms is minimal compared to the movement of the H atoms, or just about 0.1Å for the two nearest Cu atoms in the initial state. In figure 4.8 are more examples of the tunneling path shown.

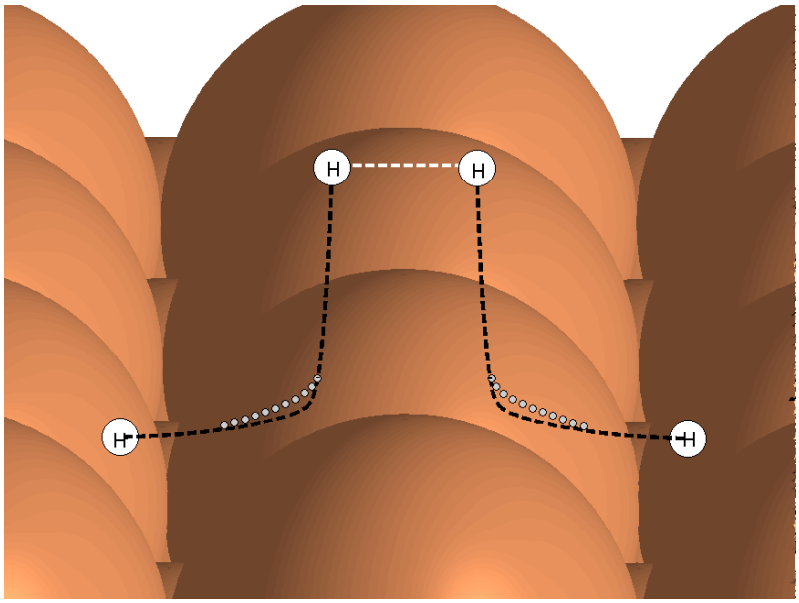

Figure 4.7: A Cu(110) surface with the MEP for associative desorption of H_2 is shown in dashed lines. The maximum tunneling path for cross-over energy equal to 0.10eV is shown in small gray circles.

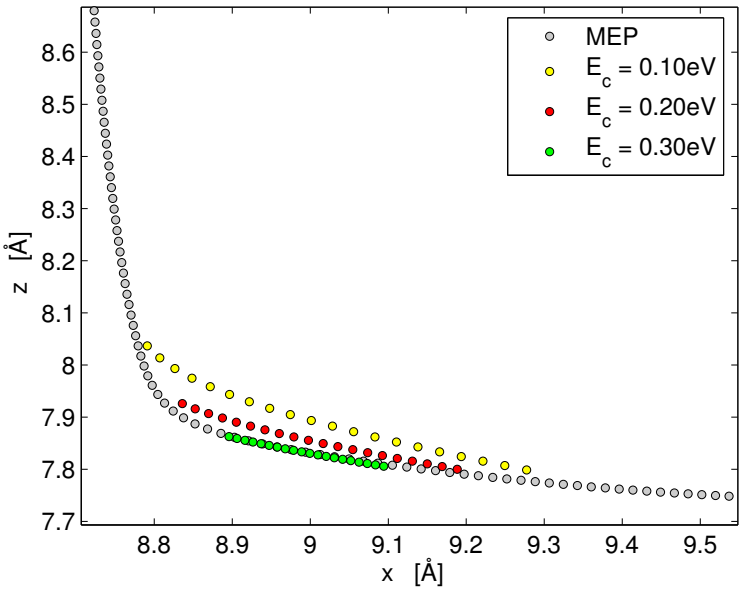

Figure 4.8: The MEP for associative desorption of H_2 and three examples of maximum tunneling paths with different cross-over energies. The coordinates represent position of one of the hydrogen atoms, position of the other atom is a reflection of the path here about the z-axis. All the paths are completely contained within the xz plane.

It has been shown that the particular parameters set employed here reproduces the physical characteristics of the interaction potential energy surface somewhat poorly [30] but the aim is only to emphasize that the method proposed to find maximum tunneling paths is applicable to systems with large number of degrees of freedom. HQTST calculations of this model have shown excellent agreement with full anharmonic rate constant calculations [31] which indicates that we might expect as good results if we use maximum tunneling paths to find the instantons.

5 WKB rate constant calculations

Calculating the quantum mechanical rate constant with HQTST method according to equation 2.22 has some numerical problems which one would like to avoid. In order to calculate the rate constant, the Hessian matrix needs to be calculated for each image in each CFP point of the MAP which requires numerous evaluations of second derivatives of the potential function. Since one is most often interested in the rate constant as a function of temperature, the alternative is to evaluate the reactive flux according to equation 2.29. This would require estimating the transmission probability P(E) and numerically involving only two integrations, one over the action integral and one over the probability.

Using the WKB formula for P(E), equation 2.25, one can estimate the transmission probability from the action integral θ. It can be done in a simple way using the MEP as a reaction path or by taking advantage of the maximum tunneling paths. This was done for the test models in chapter 4 along with calculations using other methods, described in chapter 2. When the maximum tunneling paths are used, one path is found for each cross-over energy E and a corresponding tunneling probability value $P(E)$ is calculated from the maximum action $\theta(E)$. When only the MEP is used, the integration between classical turning points is always over the MEP. Results for rate constant calculations of the Eckart+HO and LEPS+HO model are shown in figure 5.1. The method referred to as exact involves full quantum mechanical wave function calculations for the rate constant with flux-flux autocorrelation function formalism [32]. Unfortunately, the exact method is only applicable to unbound potentials, see appendix B for more details.

Since calculations using the maximum tunneling paths yield higher tunneling probability than MEP the rate constant will always be some what larger using them. The rate constant results for WKB calculations are close to exact and HQTST calculations in these examples, although a bit higher, especially for lower temperatures. Other models did not give such good comparison, results for the two models of a wire with Gaussian shaped impurities are shown in figure 5.2.

The rate constant results for the calculation using P(E) according to WKB clearly have some inaccuracies, this might not be surprising since the method applied is defined as a one dimensional method. In next section the use of a multi-dimensional extension to the tunneling paths is proposed in hope to get a better agreement

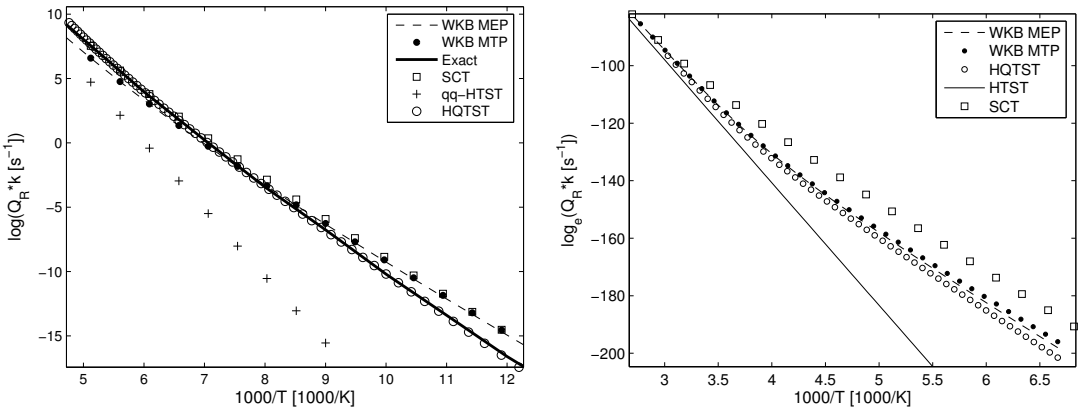

Figure 5.1: Reactive flux for the Eckart+HO potential energy function on left and the LEPS+HO function on right. WKB MEP stands for calculations of WKB rate constant using the minimum energy path and WKB MTP stands for calculations of WKB rate constant using maximum tunneling paths.

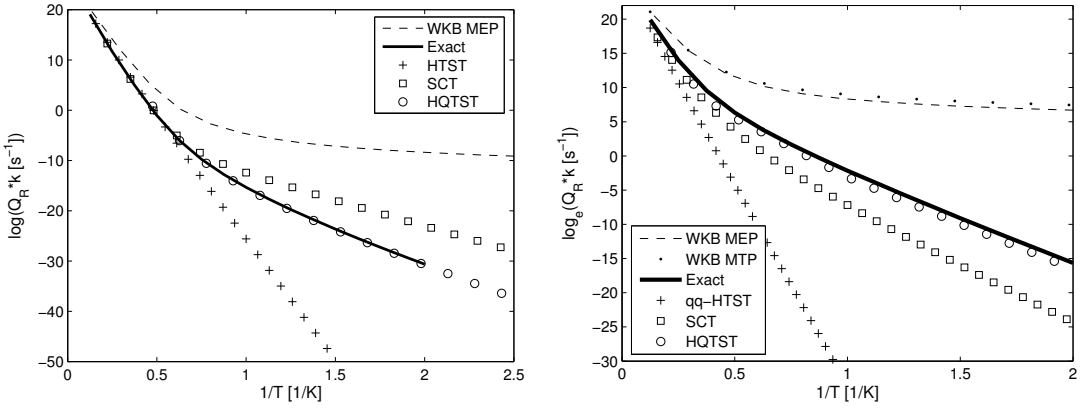

Figure 5.2: Results for the calculation of reactive flux for the potential function of a electron traveling along a model quantum nanowire with embedded impurity. Results for a single Gaussian impurity are shown on left and two symmetrically offset impurities on right.

with HQTST and exact results. However, redirecting the focus from finding P(E) to HQTST again, some computational disadvantages of HQTST described above might be prevented by finding instantons from the maximum tunneling paths as described in chapter 6.

5.1 Multi dimensional WKB

Since the goal is always to be able to handle multi dimensional system an attempt was made to propose a method for evaluating the transmission probability and the rate constant more accurately for the two dimensional test examples considered in this thesis.

This attempt involved taking into consideration all degrees of freedom and instead of having one maximum tunneling path for each energy one could think of summing over all possible paths between cross-over points. Obviously paths far away from the tunneling path will give very low tunneling probability and wont need to be considered. All paths in some specific area around the maximum tunneling path should be included.

The attempt is to find a correction to the semi-classical one dimensional WKB tunneling probability which is calculated using only the MEP.

$$P(E) = \kappa(E) P_{MEP}(E) \tag{5.1}$$

The prefactor κ can be thought of as a correction factor and should therefore somehow include the other degrees of freedom. Since the change in vibrational frequency normal to the path has not been considered in $\mathrm{P_{MEP}}$, a control potential was constructed in such a way that this vibrational frequency, or equally, the second derivative normal to the path, does not not change along the path, it is taken to be constant as in the initial state. The harmonic expansion around the initial state is kept constant along the path but the one dimensional potential barrier shape is kept the same. The control potential function can be written as an expansion around each point $\mathbf{R}_{\mathrm{MEP}}$ on the MEP.

$$V^{(0)}(\mathbf{R}) = V(\mathbf{R}_{\mathrm{MEP}}) + |\mathbf{R}_{\mathrm{MEP}} - \mathbf{R}|^2 \frac{\mu\omega_0^2}{2} \tag{5.2}$$

ω_0 is the normal vibrational frequency in the initial state and $\mathbf{R}_{\mathrm{MEP}}$ is the point on the MEP nearest to $\mathbf{R}$. For each path the probability P(E) is calculated with the correct potential function and $\mathrm{P^{(0)}(E)}$ is calculated for the same path but with the control potential function. The correction factor κ is then written as

$$\kappa(E) = \lim_{M\to\infty} \frac{\sum_{i=1}^{M} P_i(E)}{\sum_{i=1}^{M} P_i^0(E)} \tag{5.3}$$

Where M is the number of paths. We have chosen to consider only the paths with considerably high P so an extension of paths is made around the maximum tunneling path. This is done by dividing the maximum tunneling path into intervals with n

lines perpendicular to the path and calculating $P(E)$ and P^0(E) for all paths made of connection between m points on each line. A illustration of this is shown in figure 5.3.

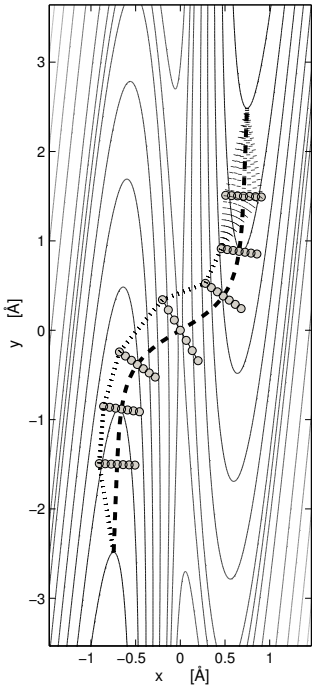

Figure 5.3: A maximum tunneling path for crossover energy Ec=0.15eV in the Eckart+HO potential energy function. Nine lines are drawn perpendicular to the path and few of the possible paths connecting the lines drawn as an example to illustrate the extension method.

In all the test models presented in chapter 4 the WKB rate constant was over estimated in comparison with exact or HQTST method, in some cases only slightly but on other cases extremely. The extension of the WKB method described here may yield a lower rate constant than WKB using MEP or maximum tunneling paths if the normal vibrational frequency increases along the path and the potential valley gets more restricted than in the initial state. If not, P^0(E) will always be lower than P(E) and κ>1, yielding higher rate constant. Two of the test models have the appropriate behavior to yield improvement of the rate constant with extension calculations, the Eckart+HO potential and the wire with two Gaussian peaks. Results of extension calculations are shown in figure 5.4.

Although the rate constant was lowered with the extension method the improvement was not major. The design of the control potential function may be lacking some important features since the correction factor does not include effects of curvature of the path itself, only potential curvature. A modification of the path sampling might also be useful.

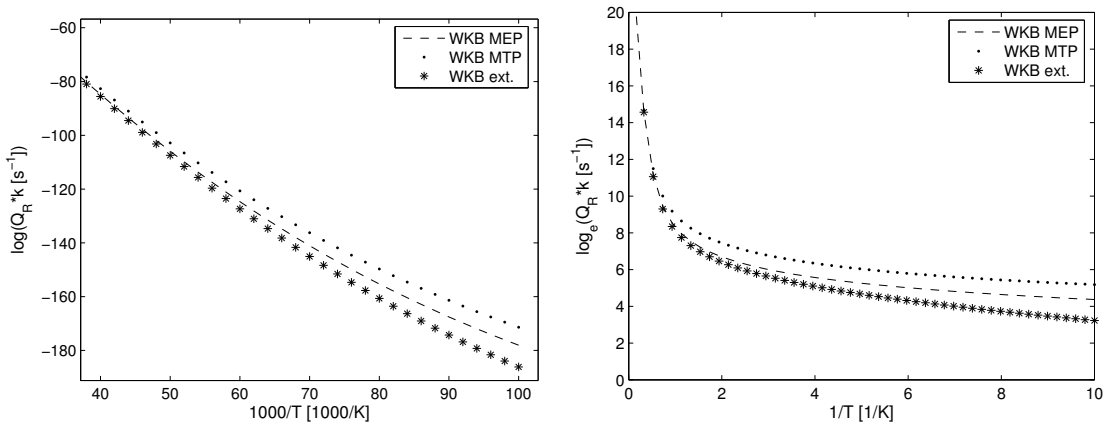

Figure 5.4: Reactive flux for the Eckart+HO potential energy function on left and the potential of a wire with two asymmetric Gaussian impurities on right. WKB MEP stands for calculations of WKB rate constant using the minimum energy path, WKB MTP stands for calculations of WKB rate constant using maximum tunneling paths and WKB ext. stands for calculations using the extension method described in this section.

Implementation of other multi-dimensional WKB methods was not considered thoroughly in this project but remains a subject of further work. On the other hand, since the maximum tunneling paths can be used instead of instantons in HQTST a lot is gained and until a more accurate formulation of the tunneling probability is achieved, possibly by implementing multi-dimensional WKB, it might be the way to proceed.

6 Instantons based on maximum tunneling paths

At first sight, the resemblance between the instanton and tunneling paths is not obvious. The instanton is a classical periodic orbit for the inverted potential corresponding to a specific temperature where the Euclidean action is minimized. The maximum tunneling paths are also periodic orbits for the inverted potential but correspond to a specific energy. It is therefore interesting to compare the instantons and the maximum tunneling paths and get a relationship between temperature dependent paths and energy dependent paths. This was first done by checking similarities between an instanton for a given temperature T and a maximum tunneling path with cross over energy E_c equal to the energy at the end points of the instanton so that both paths initiate from the same origin. An example of this is shown in figure 6.1.

The comparison revealed great similarities for all temperatures and all test model potentials, again confirming that the classical periodic orbits for the inverted potential have been found. As might be seen from figure 6.1, or more obviously from figure 6.5, the system replicas in the instanton, or the images, are not evenly distributed as the images in the maximum tunneling path. This is one of the advantages the maximum tunneling path search has over the instanton search because at low temperature the temperature dependent spring constant gets weaker and the images in the instanton tend to cluster together at the lower energy ends of the path. Calculations therefore require the addition of more and more images, as the temperature gets lower for acceptable convergence. When the images are evenly distributed as in the maximum tunneling paths this problem is avoided and the total number of images needed for convergence should be smaller at low temperatures than in the instanton method.

If the instantons search is to be replaced by finding the maximum tunneling paths one would first of all want to be able to find their corresponding temperature. The rate constant is temperature dependent but the tunneling probability in WKB is only energy dependent, see figure 6.2a for an example of the transmission probability. When calculating the rate constant according to equation 2.29 an integration is performed over the function $P(E) \cdot e^{-\beta E}$ and temperature is introduced in $\beta = 1/k_B T$. This integrand has the form of a single peak with Gaussian distribution around it,

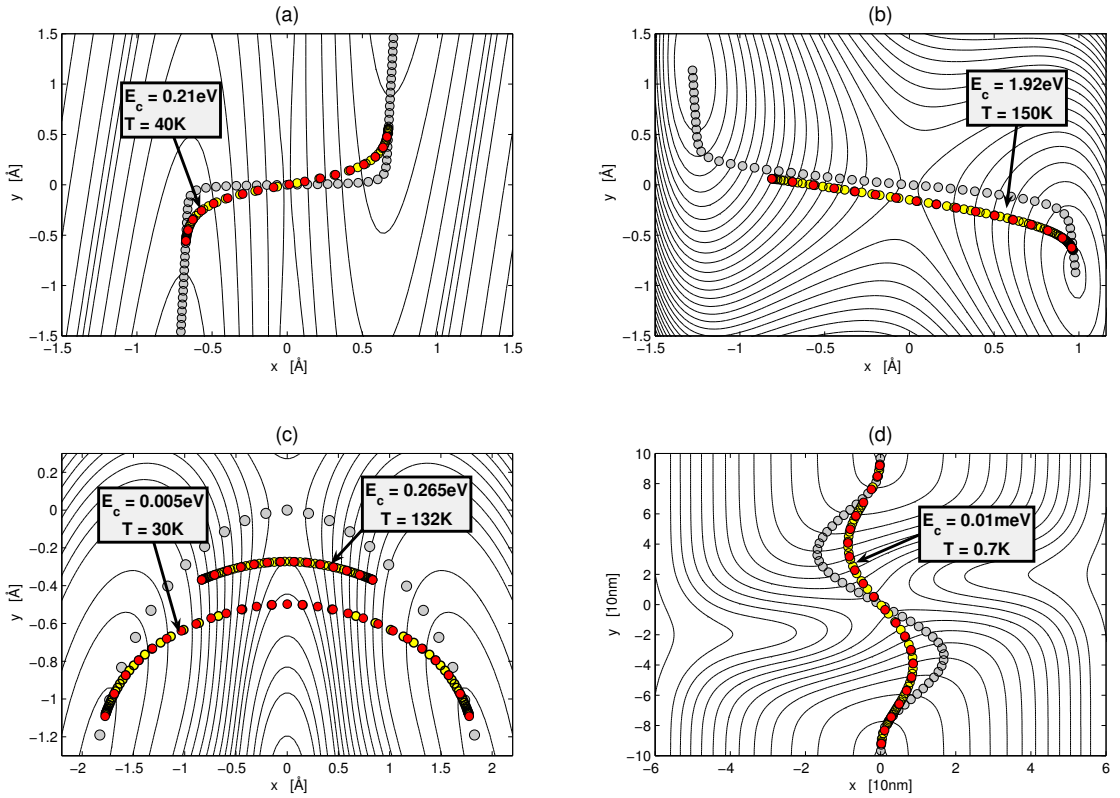

Figure 6.1: Resemblance of an instanton for a specific temperature and a maximum tunneling path for a specific energy, four different potential functions are shown. The maximum tunneling paths are shown in red and the instantons are shown in yellow.

similar to the function shown in figure 6.2b. Finding the energy corresponding to the maximum of the integrand function for each temperature, when $P(E)$ is calculated using the maximum tunneling paths according to equation 2.25, gives a relationship between temperature and energy. Comparing this energy to the end-point energy of the instantons also reveals some similarity as shown in figure 6.3.

The instantons tend to diverge at high temperature which could be cause of deviation between the two curves on the graphs in figure 6.3. The results show some relationship between instanton theory and WKB theory but the temperature could only be connected to the position of the peak maximum, not the shape of it or the value it self. It is obvious from the WKB rate constant results shown in chapter 5 that the integration over this peak is over estimated, in some cases severely. Again it is confirmed that the question of how to accurately approximate P(E) remains, and we redirect the focus of rate constant calculation from the exact equation 2.29 to HQTST.

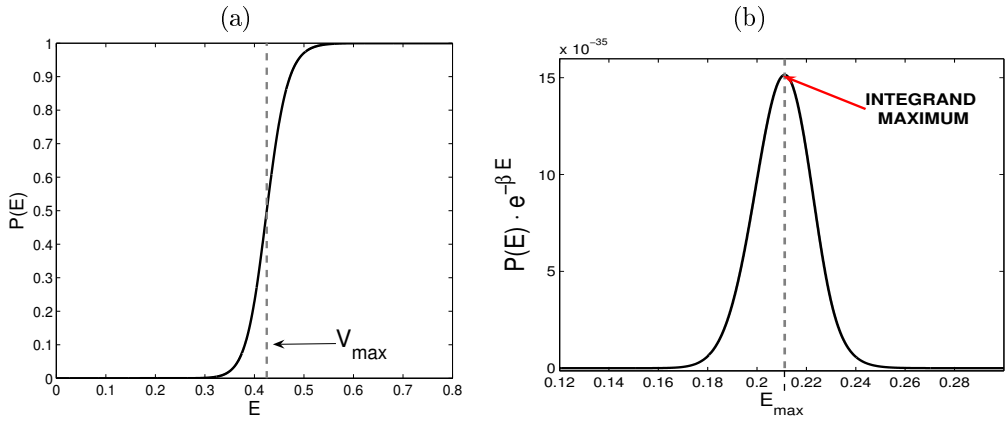

Figure 6.2: (a) An example of a transmission probability for a barrier with maximum height V_{max} as a function of energy. (b) An example of the integrand function $P(E) \cdot e^{-\beta E}$ used to calculate the quantum mechanical rate constant. Here, P(E) is calculated with WKB using maximum tunneling paths and the temperature is 40K. The energy corresponding to the peak maximum is also the energy of end points in an instanton for this temperature.

6.1 Finding instanton temperature and distribution

The graphs shown in figure 6.3 only gives some numerical indication of the relationship of temperature and energy. An analytical relationship would be preferable. This is possible by classically calculating the time τ of the periodic orbit on the inverted potential. Since

$$\tau = \beta\hbar = \frac{\hbar}{k_B T} \Rightarrow T = \frac{\hbar}{k_B \tau} \tag{6.1}$$

the temperature can be found from the time of the period. The classical dynamics using the Verlet algorithm on the inverted potential is a very sensitive method as described previously in this thesis. The initial point has to be know in great accuracy to be able to get the appropriate trajectory. Running classical dynamics calculations using the force of the inverted potential but the coordinates of the tunneling path could give a way to estimate the time and retrieve the temperature. Since the path of the classical orbit is known, although not with the extreme accuracy needed to run Verlet, we don't need the information of position from the Verlet algorithm as we would if the path was unknown. Therefore it is possible to use Newton's equation F=ma to evaluate the velocity between each pair of points on the path and calculate the time it takes for the system to travel one orbit. The algorithm is based on projecting out the force causing the system to take curves and using only the force causing the system to travel along the path to calculate the time it takes to move a total of one period, see appendix C for detailed description. In this way

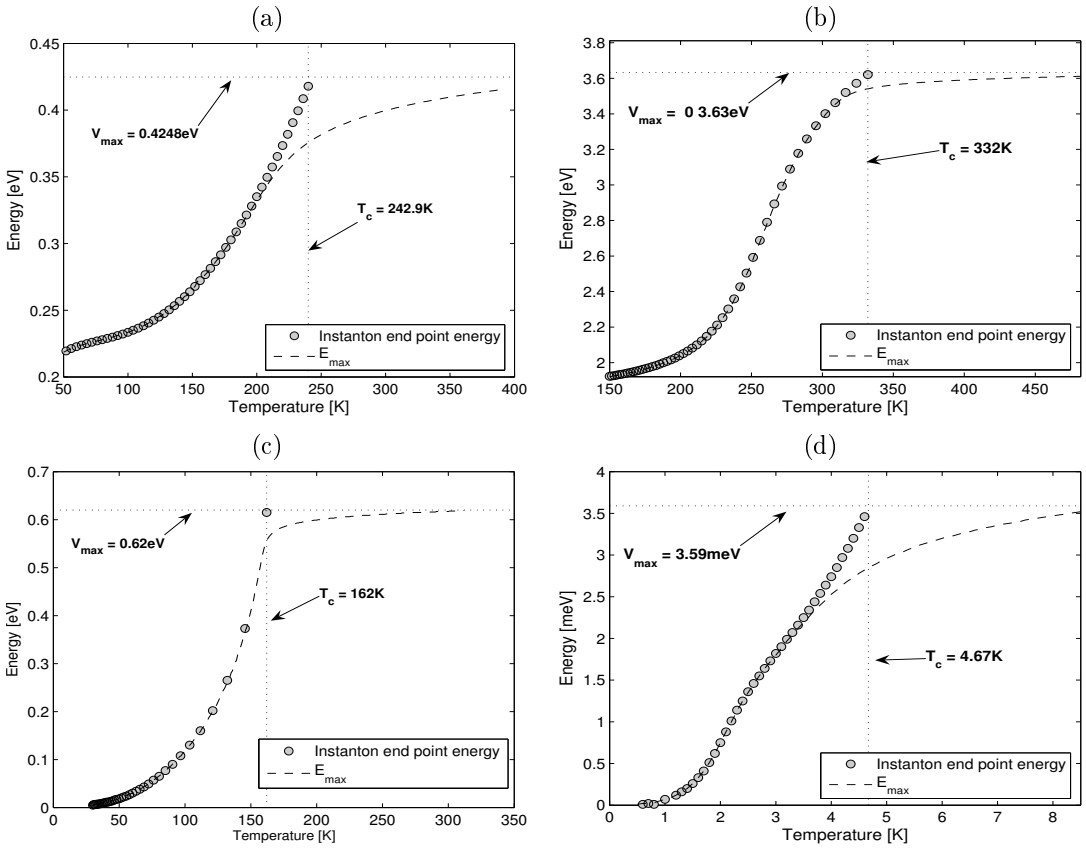

Figure 6.3: Energy of instanton end points and energy corresponding to maxima in $P^{MTP}(E)\cdot e^{-\beta E}$ versus temperature. V_{max} is the potential barrier height and T_c is the crossover temperature. (a) corresponds to Eckart+HO potential, (b) is LEPS+HO potential, (c) is constant MEP curvature potential and (d) is the potential of a nanowire with two asymmetric Gaussian peak impurities.

the task of time evaluation has been formulated into a one dimensional trajectory, regardless of the dimension of the potential function.

Using this simple algorithm to find the classical period time and using equation 6.1 to get the temperature does not require any new calculation of the potential or it's derivatives because the force of each image is already known after finding the path. The path could even be found with relatively few evenly distributed images and interpolation of the path and the force would give better accuracy of the temperature. This method of finding the temperature was tested on the models from chapter 4 and an example of the agreement is shown in figure 6.4.

Temperature values calculated from the classical dynamics time evaluations were compared to the correct temperature of the instantons for all the test models and showed only 0.1-1% error when the number of images was relatively low ($<$50). The

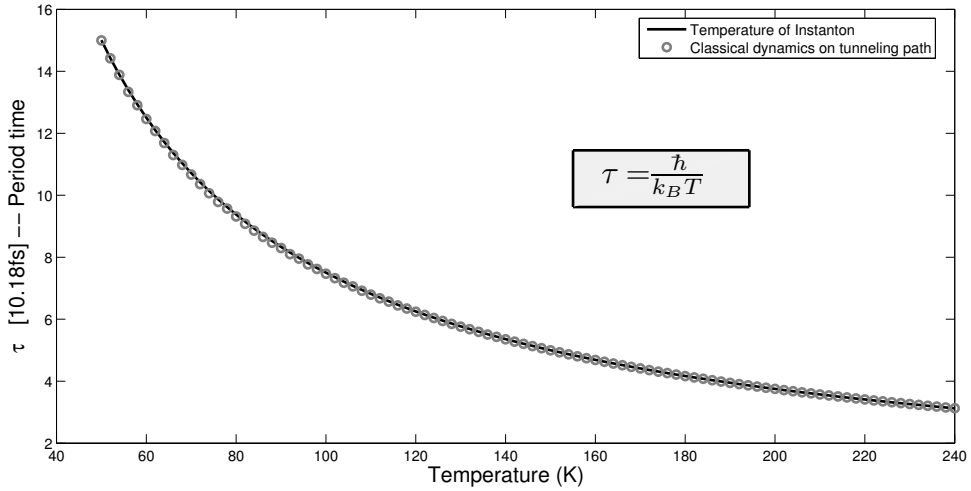

Figure 6.4: The solid line is the period time of the instantons vs. its corresponding temperature according to the equation $\tau = \frac{\hbar}{k_B T}$. The period of a tunneling path calculated with classical dynamics on the inverted potential is denoted with rings. The values are from the Eckart+HO two dimensional potential function.

number of images needed in the Eckart+HO model to get the excellent agreement of under 1% error in figure 6.4 was found to be around 20.

Although we have at this point found the path of the instanton and the temperature, the distribution of images is also important to be able to calculate the rate constant according to equation 2.22. This is because the eigenvalues needed for the prefactor calculation are found from estimating the Hessian matrix of each image. The distribution can also be found from the classical dynamic of the inverted potential as the time step is defined as $\Delta\tau = \tau/P$ where P is the number of images in a full chain. The position at each timestep can be found by interpolating the path and hence the distribution is found. The difference in image distribution is shown in figure 6.5.

Rate constant calculations using HQTST with and without using maximum tunneling paths to find the instantons were performed on the test models in chapter 4 and showed excellent agreement, with typical deviation under 1% in $log_e(Q_R k)$ values. Results for the Eckart+HO model are shown as an example in figure 6.6.

Now it has been shown that the maximum tunneling paths can replace the instantons and computational effort of the rate constant calculation can be lowered. Two things will especially contribute to this enhancement, lowered number of images, at least for low temperatures, and the search for an accurate saddle point will not be necessary. All of this resulting in fewer force calls which is highly beneficial when using first principle forces for example for density functional theory (DFT) as is most often the case when handling large systems with many degrees of freedom. Further lowering of computational effort might even be possible by calculating the Hessian matrix in

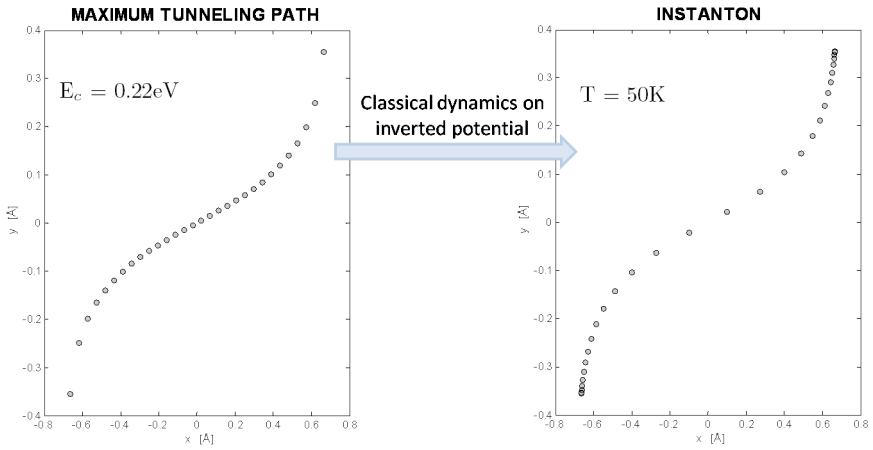

Figure 6.5: With classical dynamics run on a maximum tunneling path using inverted potential, the temperature of an instanton and its distribution of images can be found.

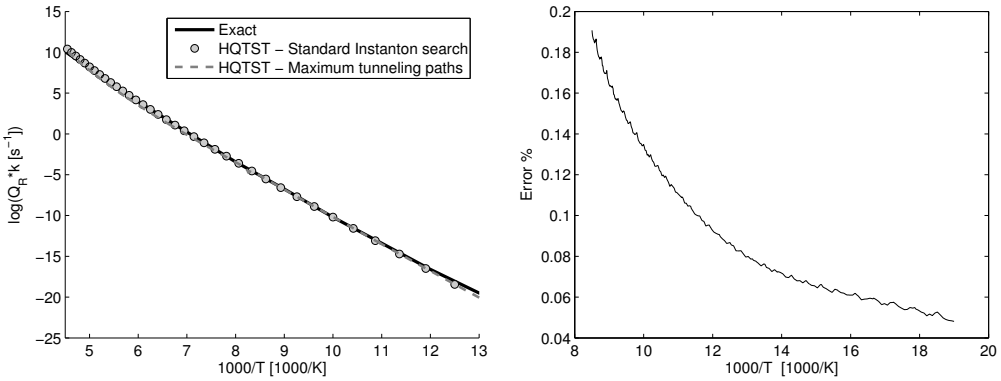

Figure 6.6: (a) Reactive flux calculated with HQTST method for the Eckart+HO two dimensional test model. The black solid line refers to full quantum mechanical wave function calculations for the rate constant, the circles represent former used HQTST method where instantons are found using the minimum mode method and the dashed gray line represents HQTST calculations were the instantons were based on maximum tunneling paths. (b) % Error with respect to exact results.

relatively few images, evenly distributed, and interpolating the second derivatives along the path and in that way increasing the number of images without new force calls.

7 Conclusions

The aim of this thesis was to develop a method for finding maximum tunneling paths that could be implemented in system of many degrees of freedom, with hope to give an insight in quantum rate constant calculations. Previous calculations of quantum rate constants have in many cases relied on the development of analytical potential energy surfaces. Such an approach is limited to systems with only very few degrees of freedom but density functional theory (DFT) calculations can offer atomic forces from first principles method for systems with hundreds of degrees of freedom. As a by-product of this project a general path optimization method was proposed for minimizing a functional dependent on a function of many variables. The path optimization method was showed to succeed for two different functionals, one simple test case and the functional representing the action of a system on a potential surface. The paths with lowest action gives highest tunneling probability. It was shown with various checks that the paths found actually yield the lowest value of the action as intended. The method was tested on various analytical test examples, both two- and three-dimensional potential energy functions and succeeded.

The paths of least action for a given system are classical periodic orbits for the inverted potential of the system. It was shown by running classical trajectories that the resulting paths from the optimization are in fact such periodic orbits but classical dynamics such as Verlet algorithm require in general extremely high accuracy of an initial coordinate to find these orbits.

The most widely used method for calculating quantum mechanical rate constants is the instanton theory, based on Feynman path integrals, which relies up on finding a quantum mechanical analog to the classical minimum energy path of a potential surface and a corresponding saddle point, called the instanton. The instantons are temperature dependent chains of system replicas and correspond to minimum Euclidean action, it is shown in this thesis that the maximum tunneling paths found using the optimization procedure presented are in fact the paths of the instantons, but they are defined to correspond to the cross-over energy of the classical turning points. A suggestion is made how the instanton can be replaced by the maximum tunneling paths as to avoid computational effort. The temperature dependence and image distribution can be found by running simple classical dynamics on the inverted potential, using the coordinates of the paths.

There are two important advantages of the maximum tunneling path method over the previously used instanton search, one is the free choice of distribution of images in the tunneling path which makes faster convergence at lower temperatures possible. At low temperatures the spring constant between system replicas in the instanton get weaker and the instantons tend to slip into the potential minima and cluster together. The images in the maximum tunneling path can be distributed in any way wanted, it was described in this thesis how the use of springs as in NEB can evenly distribute them and then the number of images needed for convergence is not increased significantly at low temperatures since these spring constants are not temperature dependent as the ones of the instantons. The other advantage is that there is no need for search of an accurate classical saddle point. This search is extremely important when finding the instanton using the minimum mode method [31] as the classical saddle point is the starting point of the construction of the quantum mechanical saddle point, the instanton. No requirement of specific features of the initial guess of a maximum tunneling path is made.

The one dimensional WKB approximation for the transmission probability P(E) was tested using both the contribution of just the MEP on one hand, and a maximum tunneling path for each energy on the other. Results showed that the probability was over estimated using this method in all the test examples considered, some showed only slight deviation from exact method and instanton method but other showed extreme deviation. It is therefore clear that if the quantum rate constant is to be evaluated by integrating over the transmission probability the question of how to accurately approximate P(E) still remains. This procedure of two integrations, one over the action and one over the transmission probability, is in many ways preferable over other more computationally complicated methods with many evaluations of second derivatives. Possible further work is the procedure of finding maximum tunneling paths in to the SCT method as the effect of curvature of the path would then be included in the effective mass. Considering successive multi dimensional WKB methods might also give insight to this topic.

As a further project, the full replacement of instanton search by the maximum tunneling path method proposed here will be continued. Improvement of the method by interpolation of second derivatives will be tested in hope to lower computational effort even further. Implementation to commonly used DFT codes for rate constant calculations is also a future aim.

Bibliography

[1] H. Jónsson, G. Mills, and K. W. Jacobssen, in *Classical and quantum dynamics in condensed phase simulations*, edited by B. J. Berne, G. Ciccotti, and D. F. Coker (World Scientific Publishing Co., Singapore, 1998), p. 385,

[2] R. P. Feynman, *Statistical Mechanics - A set of lectures* (The Benjamin/Cummings Publishing Company, USA, 1982).

[3] R. P. Feynman and A. R. Hibbs, *Quantum Mechanics and Path Integrals* (McGraw-Hill Book Company, ADDRESS, 1965).

[4] G. Mills, G. K. Shenter, D. E. Makarov, and H. Jónsson, Chemical Physics Letters **278**, 91 (1997).

[5] C. G. Callan and S. Coleman, Phys. Rev. D **16**, 1762 (1977).

[6] M. J. Gillan, J. Phys. C: Solid State Physics **20**, 3621 (1987).

[7] M. Messina, G. Schenter, and B. C. Garrett, J. Chem. Phys. **103**, 3430 (1995),

[8] B. C. Garrett and D. G. Trhular, J. Phys. Chem. **83**, 2921 (1979), the barrier jafna o.fl.

[9] L. Brillouin, Comptes Rendus **183**, 24 (1926).

[10] H. A. Kramers, Zeits. f. Phys. **39**, 828 (1926).

[11] G. Wentzel, Zeits. f. Phys. **38**, 518 (1926).

[12] *Quantum mechanics*, edited by L. I. Schiff (McGraw-Hill Book Company, New York, 1968).

[13] W. H. Miller, J. Phys. Chem. **62**, 1899 (1975),

[14] J. Zamastil, Phys. Rev. A **72**, 24101 (2005).

[15] Z. H. Huang, T. E. Feuchtwang, P. H. Cutler, and E. Kazes, Phys. Rev. A **41**, 32 (1990).

[16] A. Auerbach and S. Kivelson, Nuclear Physics B **257**, 799 (1985).

[17] R. T. Skodje, D. G. Truhlar, and B. C. Garrett, J. Phys. Chem. **85**, 3019 (1981),

[18] R. T. Skodje and D. G. Truhlar, J. Chem. Phys **77**, 5955 (1982).

[19] E. Weinan, R. Weiqing, and E. Vanden-Eijnden, Phys. Rev. B **66**, 52301 (2002).

[20] L. Verlet, Phys. Rev. **159**, 98 (1967).

[21] G. H. Jóhannesson and H. Jónsson, J. Chem. Phys. **115**, 9644 (2001).

[22] R. P. McRae, G. K. Schenter, and B. C. Garrett, J. Chem. Phys. **97**, 7392 (1992).

[23] J. H. Bárdarson, I. Magnúsdottir, G. Gudmundsdóttir, A. M. C.-S. Tang, and V. Gudmundsson, Phys. Rev. B **70**, 245308 (2004).

[24] V. Guðmundsson, G. Guðmundsdóttir, J. H. Bárðarson, I. Magnúsdóttir, C.-S. Tang, and A. Manolescu, Eur. Phys. J. B **45**, 339 (2005).

[25] V. Guðmundsson, Y. Y. Lin, C.-S. Tang, V. Moldoveanu, J. H. Bárdarson, and A. Manolescu, Phys. Rev. B **71**, 235302 (2005).

[26] J. C. Polanyi and W. H. Wong, J. Chem. Phys. **51**, 1439 (1969).

[27] G. Alefeld, R. M. Cotts, K. W. Kehr, H. Kronmuller, H. Peisl, A. Seeger, K. Sköld, T. Springer, A. C. Switendick, J. Völk, F. E. Wagner, H. Wagner, W. E. Wallace, and G. Wortmann, in *Hydrogen in Metals I: Basic Properties*, Vol. 28 of *Topics in Applied Physics*, edited by G. Alefeld and J. Völk (Springer-Verlag, Germany, 1978).

[28] G. Mills, H. Jónsson, and G. K. Schenter, Surf. Sci. **324**, 305 (1995).

[29] M. S. Daw and M. I. Baskes, Phys. Rev. B **29**, 6443 (1984).

[30] C. Bae, D. L. Freeman, J. D. Doll, G. Kresse, and J. Hafner, J. Chem. Phys. **113**, 6926 (2000).

[31] A. Arnaldsson, Ph.D. thesis, University of Washington, 2007.

[32] W. H. Miller, S. Schwartz, and J. W. Tromp, J. Chem. Phys **79**, 4889 (1983),

Appendix A: Derivation of action functional

Consider a particle of mass m moving in one dimension, under influence of a potential $V(x)$. We can describe the classical motion of the particle either via a Hamiltonian or a Lagrangian.

$$H(x,p) = \frac{p^2}{2m} + V(x) \quad , \qquad L(x,\dot{x}) = \frac{1}{2}m\dot{x}^2 - V(x) \tag{A.1}$$

The equations of motion are respectively the Hamilton equations or the Euler-Lagrange equations

$$\dot{x} = \frac{\partial H}{\partial p} \qquad \dot{p} = -\frac{\partial H}{\partial x} \quad , \qquad \frac{d}{dt}\frac{\partial L}{\partial \dot{x}} - \frac{\partial L}{\partial x} = 0 \tag{A.2}$$

The Hamiltonian and Lagrangian are related via a Legendre transformation:

$$H(x,p) = p\dot{x} - L(x,\dot{x}) \quad , \qquad p = \frac{\partial L}{\partial \dot{x}} \tag{A.3}$$

$$L(x,\dot{x}) = p\dot{x} - H(x,p) \quad , \qquad \dot{x} = \frac{\partial H}{\partial p} \tag{A.4}$$

Consider a path $x(t)$ that starts at position x_0 at time t_0 and ends at position x_n at time t_n. The action functional S is defined as the integral over time of the Lagrangian $L(x,\dot{x})$

$$S(x,t) = \int L(x,\dot{x})dt \tag{A.5}$$

Evaluating the action functional for the classical trajectory $x(t)$ of energy E, we put A.4 in to A.5 and get

$$S = \int_{\substack{\text{Classical path} \\ (x_0,t0)\rightarrow(x_n,tn)}} (p\frac{dx}{dt} - H)dt = \int_{x_0}^{x_n} p(x)dx - E(t_n - t_0) \tag{A.6}$$

For a classical trajectory with energy E, the momentum p can be solved as a function of position x via

$$H(x,p) = E \quad \rightarrow \quad p(x) = \sqrt{2m(E - V(x))} \tag{A.7}$$

The classical trajectory is related to a tunneling trajectory because for quantum tunneling we have $E < V$ and the Schrödinger equation allows for solutions in which $p(x)$ takes an imaginary values. This is equal to motion during an imaginary time interval, or replacing t by it which has the same effect as flipping the sign of the potential $V(x)$ in the Euler-Lagrange equations. The imaginary action integral is then defined as

$$S(E) = \int_{x_0}^{x_n} \sqrt{2m(E - V(x))}dx \tag{A.8}$$

Appendix B: Exact method for rate constant calculations

The rate constant method referred to as exact involves full quantum mechanical wave function calculations for the rate constant with flux-flux autocorrelation function formalism[32]. The equation for the exact rate constant is

$$Q_R k = \int_0^\infty C_f(t) dt \tag{B.1}$$

where Q_R is the partition function for the reactant state and $C_f(t)$ is the flux-flux correlation function. A discrete system Hamiltonian is constructed on a uniform grid of n_x points along the x-coordinate and n_y along the y-coordinate. The corresponding matrix representation is diagonalized to produce the eigenfunctions and eigenvalues ($\phi_i(x,y)$ and ϵ_i respectively with $i = 1, ..., n_x n_z$). In this representation the correlation function becomes

$$C_f(t) = \sum_{i,j}^{n_x n_y} exp\left(-\frac{\epsilon_i + \epsilon_j}{2k_B T}\right) cos\left(\frac{\epsilon_i - \epsilon_j}{\hbar} t\right) \left(\frac{\hbar}{2m}\right)^2 \int |\psi_i' \psi_j - \psi_i \psi_j'|^2 \tag{B.2}$$

where in the last integral, the wave functions are evaluated at the classical transition state and their derivatives estimated along the reaction coordinate. The integration extends over all other degrees of freedom, except the reaction coordinate. By integrating the correlation function according to equation B.1, the rate expression becomes

$$Q_R k = \lim_{t\to\infty} \sum_{i,j}^{n_x n_y} exp\left(-\frac{\epsilon_i + \epsilon_j}{2k_B T}\right) \frac{sin((\epsilon_i + \epsilon_j)t/\hbar)}{\epsilon_i - \epsilon_j} \left(\frac{\hbar}{2m}\right)^2 \int |\psi_i' \psi_j - \psi_i \psi_j'|^2 \tag{B.3}$$

Appendix C: Algorithm for finding the travelling time along a given path

Starting with the fact that a system with mass m will travel along a given path defined as a collection of coordinate vectors $\mathbf{R} = \{\mathbf{R}_1, \mathbf{R}_2, ..., \mathbf{R}_n\}$. Assuming that the force acting on the system, $\mathbf{F}$, is known at all points on the path, the component of $\mathbf{F}$ parallel to the path in point $\mathbf{R}_i$ is

$$F_i^{\parallel} = |(\mathbf{F}_i \cdot \widehat{\boldsymbol{\tau}}_i)\widehat{\boldsymbol{\tau}}_i| \tag{C.1}$$

where $\widehat{\boldsymbol{\tau}}_i$ is the unit tangent vector. This is the force causing the system to move along the path, the perpendicular component would cause the system to curve. The distance from point $\mathbf{R}_{i+1}$ to the next point on the path is

$$d_i = |\mathbf{R}_{i+1} - \mathbf{R}_i| \tag{C.2}$$

and the task is converted in to solving the motion of a mass m along a straight line. The acceleration is found by Newton's equation

$$a_i = \frac{F_i^{\parallel}}{m} \tag{C.3}$$

and knowing the initial velocity, v_0, the travel time t_i between each pair of points $\mathbf{R}_i$ and $\mathbf{R}_{i+1}$ is found by solving

$$d_i = v_i t_i + \frac{a_i t_i^2}{2} \tag{C.4}$$

which gives

$$t_i = \frac{\pm\sqrt{v_i^2 + 2a_i d_i} - v_i}{a_i} \tag{C.5}$$

where the positive square root gives the physical solution of increasing time. Now, the velocity in the next point $\mathbf{R}_{i+1}$ is calculated by

$$v_{i+1} = a_i t_i + v_i \tag{C.6}$$

and the total traveling time along the path is the sum of the time between all points:

$$t_{\text{tot}} = \sum_{i=1}^{n} t_i \tag{C.7}$$